EJN European Journal of Neuroscience

FENS Federation of European Neuroscience Societies

European Journal of Neuroscience, Vol. 40, pp. 2948–2962, 2014 doi:10.1111/ejn.12664

BEHAVIORAL NEUROSCIENCE

Excitation and inhibition in recurrent networks mediate collision avoidance in *Xenopus* tadpoles

Arseny S. Khakhalin, David Koren, Jenny Gu, Heng Xu and Carlos D. Aizenman
Department of Neuroscience, Brown University, Box G-LN, Providence, RI 02912, USA

Keywords: looming stimuli, optic tectum, sensorimotor transformation, vision

Abstract

Information processing in the vertebrate brain is thought to be mediated through distributed neural networks, but it is still unclear how sensory stimuli are encoded and detected by these networks, and what role synaptic inhibition plays in this process. Here we used a collision avoidance behavior in *Xenopus* tadpoles as a model for stimulus discrimination and recognition. We showed that the visual system of the tadpole is selective for behaviorally relevant looming stimuli, and that the detection of these stimuli first occurs in the optic tectum. By comparing visually guided behavior, optic nerve recordings, excitatory and inhibitory synaptic currents, and the spike output of tectal neurons, we showed that collision detection in the tadpole relies on the emergent properties of distributed recurrent networks within the tectum. We found that synaptic inhibition was temporally correlated with excitation, and did not actively sculpt stimulus selectivity, but rather it regulated the amount of integration between direct inputs from the retina and recurrent inputs from the tectum. Both pharmacological suppression and enhancement of synaptic inhibition disrupted emergent selectivity for looming stimuli. Taken together these findings suggested that, by regulating the amount of network activity, inhibition plays a critical role in maintaining selective sensitivity to behaviorally-relevant visual stimuli.

Introduction

A central question in neuroscience is how the activity of individual neurons can serve as a substrate for such emergent phenomena as perception, cognition, or executive function. It is presumed that sensory stimuli and behavioral programs are encoded by distributed neural networks (Reid, 2012), but in most cases the logic of this encoding is still unknown. In particular, it is unclear whether the main role of inhibitory circuits in the brain is to dynamically modulate and balance the activity of excitatory circuits, or whether they also maintain information transfer, and actively sculpt the output of microcircuitry modules (Isaacson & Scanziani, 2011), such as cortical and collicular columns.

Visually guided collision avoidance in *Xenopus* tadpoles (Dong *et al.*, 2009) is a robust experimental model, in which both sensory inputs and motor outputs can be easily accessed and manipulated. From a computational point of view, this behavior can be considered a case of stimulus classification (Gabbiani *et al.*, 2004) or decision making (Brembs, 2011), as animals need to categorise objects around them into two broad categories: those that approach them at an interception trajectory, and need to be avoided, and those that should be ignored (Fotowat & Gabbiani, 2011). Collision detection is universal among animals that rely on vision, from arthropods (Card, 2012; Herberholz & Marquart, 2012) to fish (Colwill & Creton, 2011), birds (Frost & Sun, 2004), and mammals (Liu *et al.*, 2011), including humans (Komban *et al.*, 2011).

In tadpoles, avoidance behavior is thought to be maintained by a mostly feed-forward network (Fig. 1), with the shortest path connecting primary afferents (rods and cones) to the effectors (muscles) being only five neural cells or six synapses long (Holt & Harris, 1983; Dong *et al.*, 2009). In both fish and amphibians the motor command is likely to be finalised at the level of reticulospinal neurons in the hindbrain (Perrins *et al.*, 2002; Preuss *et al.*, 2006; Orger *et al.*, 2008), suggesting that stimulus categorisation has to happen upstream of the hindbrain neurons, in the retina, in the optic tectum (OT), or during synaptic transmission from the OT to the hindbrain (Fig. 1). Similar to the cerebral cortex, the tadpole OT has a layered structure (Lazar, 1973) with a network of recurrently interconnected glutamatergic excitatory cells (Pratt *et al.*, 2008), and a smaller sub-network of γ-aminobutyric acid (GABA)ergic cells (Akerman & Cline, 2007; Miraucourt *et al.*, 2012). Synapses in the OT are plastic (Vislay-Meltzer *et al.*, 2006; Shen *et al.*, 2014), and resemble cortical synapses from both the molecular (Pratt & Khakhalin, 2013), and developmental (Wu *et al.*, 1996) points of view, making the OT a promising model for studying general aspects of vertebrate neural system organisation.

In this study we combine behavioral analyses with *in vivo* electrophysiological recordings, first, to identify the circuitry underlying looming stimuli detection in the tadpole brain, and, second, to probe the role of synaptic inhibition in collision detection. Answering these questions would provide perspective on the relationship between the elementary computational processes performed at the microcircuit level, and the emergent phenomena in the brain.

Correspondence: Carlos D. Aizenman, as above.
E-mail: Carlos_Aizenman@brown.edu

Received 3 March 2014, revised 23 April 2014, accepted 28 May 2014

© 2014 Federation of European Neuroscience Societies and John Wiley & Sons Ltd

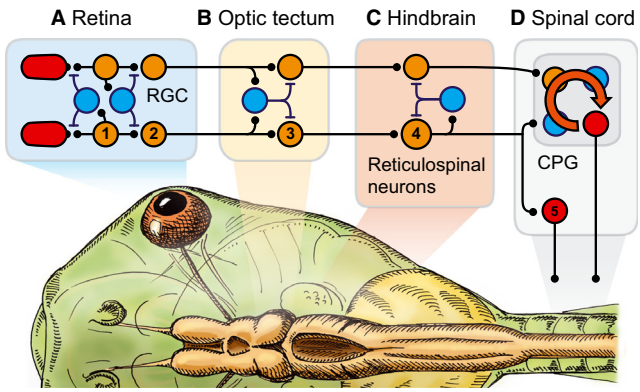

FIG. 1. Simplified diagram of the feed-forward network mediating visually-guided escape behaviors. Excitatory synapses are shown as small circles and inhibitory synapses as t-shaped lines; most feed-back and recurrent connections are not shown. Photoreceptors in the retina (A) connect to bipolar cells (1) that synapse onto RGCs (2). In premetamorphic tadpoles RGCs send axons predominantly to the contralateral OT (B) (Steedman *et al.*, 1979), a midbrain structure that is homologous to the mammalian superior colliculus (Hiramoto & Cline, 2009), and that is required for collision avoidance behavior (Dong *et al.*, 2009). In the tectum, RGC axons form direct retinotopic connections onto tectal cells (3) (Bollmann & Engert, 2009). Tectal cells project to the hindbrain (C) and synapse onto reticulospinal neurons (4), such as the Mauthner cell (Will, 1991) and its homologs (Straka *et al.*, 2001). Reticulospinal neurons control swimming by projecting to motor neurons (5) and central pattern generators (CPGs) in the spinal cord (D) (Roberts *et al.*, 2000).

Materials and methods

Data presentation and abbreviations

In the text, average values are given with SD (mean ± SD), whereas the figures show median values with 25–75% interquartile ranges, unless explicitly indicated otherwise. Sample sizes are reported as $n = X$, $N = Y$, where n is the number of cells, and N is the number of animals. When results of statistical tests are reported, P_{MW} stands for a Mann–Whitney test, P_W for a Wilcoxon signed-rank test, P_{ANOVA} for an ANOVA test, and P_{Corr} for a Student's test on the Pearson correlation coefficient (r).

Behavioral experiments in freely-swimming animals

All animal experiments were performed in accordance to IACUC standards (the Brown University Institutional Animal Care and Use Committee). Wild-type *Xenopus laevis* tadpoles were raised in 10% Steinberg's solution at 18–21 °C, on a 12 h/12 h light/dark cycle. All experiments (both behavioral and electrophysiological) were performed on tadpoles at developmental stages 48–49 (Nieuwkoop & Faber, 1994) (11–17 days post-fertilisation, depending on the temperature). Animals were tested in a clear plastic Petri dish (4.25 cm in diameter) filled to a depth of 1 cm with rearing medium at 18 °C. The dish was put on top of a CRT monitor screen (maximum luminance 57 cd/m^2, minimum luminance 0.3 cd/m^2; Ultrascan 1600 SH Series; Dell), and the monitor was screened from all sides with an opaque cloth. Stimuli were generated by a custom-written MATLAB program (MathWorks, Natick, MA, USA), which used the Psychophysics Toolbox (Brainard, 1997). A black circle (radius ranging from 0.13 to 0.56 cm) was projected in the center of the dish; every 30 s this circle was manually targeted and sent towards the tadpole at a speed ranging from 1.5 to 6 cm/s. Only approach trials in which the animal was swimming within 1 s before the encounter with the circle were included in the data set. In a separate set of experiments the circles were triggered to appear near the tadpole instantaneously, without an approach. All experiments were performed in the morning, as the animals were less responsive in the afternoon. Each testing session lasted for 5 min, and each animal was tested in no more than three sessions. Sessions were recorded with a color camera (SCB 2001; Samsung, Seoul, Korea) at 30 frames/s, and the positions of both the tadpole and the circle were tracked in Noldus EthoVision XT (Noldus Information Technology, Leesburg, VA, USA). Tracks were corrected manually, and exported for further analysis.

The geometry of collisions and escape trajectories was analysed in Matlab (see Fig. 2A for an example of a trajectory from a single experiment). For all collisions that triggered an escape we manually found the last frame before a rapid acceleration ('startle point'), and the last frame at which the original swimming direction could be estimated unambiguously ('turn point'). As Noldus EthoVision did not report the tadpole orientation in space, we estimated the pre-collision orientation of the animal by linearly fitting its position across five consecutive frames before the 'turn point'. The 'turn point' was chosen a few frames before the 'startle point' (average of five frames), as animals stopped swimming immediately before performing the C-turn maneuver (Hale *et al.*, 2002). To compare collision events that triggered an escape ('successes') with those that did not ('failures') we had to mark-up 'failures' similarly to 'successes', choosing a point corresponding to a 'startle point' in trajectories that did not in fact have startles in them. To do this we first extrapolated the tadpole and circle trajectories beyond the 'startle point' for 'successes', and estimated that most tadpoles would have passed at the shortest distance from the circle center eight frames after the 'startle point' (median time from the 'startle point' to the estimated closest approach, 234 ms; interquartile range, 33–300 ms). Accordingly, for 'failures' we measured the key collision parameters at the point that preceded the point of closest approach by eight frames. We used this 'startle point' (either actual or estimated) to measure (see Fig. 2B): swimming speed and direction immediately before (−422 to −155 ms) and after (167–267 ms) this point (these were used to estimate turning angles β and γ); angle between the tadpole swimming direction and the direction to the center of the circle (α); distance to the circle center; and angular size of the circle (θ). We also measured the rostrocaudal position along the tadpole's body axis at which the circle was targeting in the tadpole's local coordinates (rostrocaudal 'offset'). We attempted to estimate the solid angle covered by the circle, but analysis results based on these estimations were not qualitatively different from those based on the planar angle, and are not reported here.

Experiments in partially immobilised animals

A 2% solution of low-melt agarose was heated on the stove until boiling, and cooled down to about 40 °C. Tadpoles were anesthetised in 0.02% MS-222 for 10 min, rinsed in Steinberg's solution, and transferred to a Sylgard block (Dow Corning, Midland, MI, USA) glued inside a Petri dish. Excess solution was removed with a plastic pipette, and agarose was applied, in two layers, completely covering the tadpole. After leaving the gel to solidify for 5 min, one eye, the mouth, and the tail were cleared from the gel (Fig. 3A), and the dish was filled with rearing solution. The Petri dish was placed in a light-sealed box, containing an array of infrared LEDs (JG-830; Shenzhen Shuangjinge Technology Co., Ltd, China), a set of green LEDs that provided ambient illumination (tadpoles were less responsive when placed in complete darkness), and a custom-built optical stimulation device (see below). The tadpoles were

© 2014 Federation of European Neuroscience Societies and John Wiley & Sons Ltd

filmed with a Motion Pro X3 high-speed infrared camera (Redlake MASD LLC, San Diego, CA, USA) at 100 frames/s for 2 s after the stimulus onset, with videos acquired in Motion Studio (IDT Inc., Tallahasse, FL, USA). Stimulation and data acquisition were triggered every 45 s by a Master-8 pulse generator (API Instruments, Jerusalem, Israel). Only videos in which tadpoles attempted 'background swimming' (tail oscillations at a frequency of 7–9 Hz) before the stimulus delivery were included in the data set. Up to 10 stimuli of each type (see below) were delivered to each tadpole, unless the animal escaped from the gel prematurely (average of 6.3 stimuli per animal per stimulus type). Videos were analysed offline, and the tail tip position was tracked manually in IMAGEJ (National Institute of Health, USA).

The angle α between the tip and the base of the tail was measured for each frame. As the tail kept oscillating at a base frequency of v_0 = 7–9 Hz before the stimulus onset, the responses could not be thresholded directly, as they were manifested as changes in oscillatory motion. To detect the response onset we used a variable $R^2 = (\alpha')^2/(2\cdot\pi v_0)^2 + \alpha^2$, which was near constant before the response, but changed when either the average tail orientation or the frequency of oscillations changed (the value corresponded to a squared radius of a circle describing the trajectory of a harmonic oscillator in its phase space, and is therefore constant for a stable sinusoidal motion at a frequency v_0). Here α' is a finite difference approximation of the angular speed. Using R^2 thresholding we classified all responses into 'successes' and 'failures', and estimated response latencies. To verify the detection, we also performed manual detection of response latencies in a blinded fashion; manual and automated estimations of both escape probabilities (per animal per stimulus), and average response latencies were highly correlated (r = 0.90, P_{Corr} = 5e−21 for probabilities; r = 0.74, P_{Corr} = 3e−43 for latencies, n = 57). For spectral analysis, a power spectrum of $\alpha(t)$ was averaged across the 0–5 Hz range (low-frequency component, corresponding to tail deflections, or 'tail-flicks'), and 12–40 Hz range (high-frequency component, corresponding to increases in tail oscillation frequency, or 'acceleration').

To reconstruct the trajectory that tadpoles tried to follow during the constrained escape response we assumed that slow tail deflections normally make swimming tadpoles turn, whereas changes in oscillation frequency change the swimming speed. We iteratively calculated the 'virtual position' of the tadpole, assuming that at each time point i it had a speed of $s = \alpha'$ (where α' is a finite difference approximation of the angular speed), and moved at a distance $s\cdot dt$ along its current orientation β. We also assumed that this orientation changed proportionally to the tail deflection angle: $\beta_{i+1} = \beta_i + k\alpha\cdot dt$. Here k is an arbitrary constant, chosen at k = 3e−4, as at this value the trajectories looked visually similar to real trajectories, and the analysis results did not change qualitatively for all values of k in the range from 5e−5 to 1e−3. This relative insensitivity to the exact value of k justifies the use of a simplified approach to trajectory reconstruction. To quantify the escape trajectories we compared the tadpole's virtual position at 1 s after the escape onset (linearly extrapolated if necessary) with the 'expected virtual position' that the tadpole would occupy in the absence of an escape response (which was estimated by linear extrapolation of the initial segment of the trajectory from t = 0 until the point of escape onset). The same calculation algorithm was applied to trials lacking an escape response, except that the median response onset latency was used. We did not attempt to calibrate or compare reconstructed 'virtual trajectories' with actual trajectories recorded in freely-swimming animals, as tail movements were often restricted in partially immobilised animals; visual stimulation only approximately replicated stimuli from swimming experiments (see below); and our data (tail tip movements) were insufficient to build an accurate kinematic model of swimming.

Electrophysiology

Animals were anesthetised in 0.02% MS-222 for 10 min, and then paralysed by pre-treatment with 20 mM tubocurarine, 0.1 mM bungarotoxin, or 2 mM pancuronium for 4 min (Dunfield & Haas, 2009), or, in early experiments, with 0.1 mM tubocurarine or 1 μM bungarotoxin introduced into the artificial cerebrospinal fluid (ACSF) in the recording chamber for the entire length of the experiment (Xu *et al.*, 2011; Dong & Aizenman, 2012). The external medium (ACSF) in the chamber contained (in mM): 115 NaCl, 4 KCl, 3 $CaCl_2$, 3 $MgCl_2$, 5 HEPES, 10 mM glucose (pH 7.2, osmolarity 255 mOsm) (Aizenman *et al.*, 2003). The animals were stabilised on a Sylgard block, carved to better hold the animal, with three dissecting pins and an overarching staple (Xu *et al.*, 2011). For recordings from the optic nerve, the nerve was surgically severed, and sucked into a broken glass micropipette filled with extracellular solution; recordings were then performed in current-clamp mode. For recordings from the OT, the tectal lobes were exposed by removing the overlying skin over the right tectum, and cutting both the caudal and frontal dorsal commissures between the tecta. The OT cells were visualised using a 60× water-immersion objective. Loose-cell-attached, and whole-cell voltage-clamp recordings were performed at room temperature (22–25 °C) using glass micropipettes (9–12 MΩ) filled with ACSF or intracellular solution, respectively [the latter containing (in mM): 90 Cs-methanesulfonate, 5 $MgCl_2$, 20 Tetraethylammonium, 10 EGTA, 20 HEPES, 2 ATP, 0.3 GTP (pH 7.2, osmolarity 255 mOsm)]. Cells were randomly sampled from the middle half of the tectum. Cells that looked larger than the main population of OT cells were not approached, to avoid recording from mesencephalic trigeminal neurons (Pratt & Aizenman, 2009). For loose-cell-attached recordings cells were approached in current-clamp mode, and negative suction was carefully applied until clear spikes became visible above the background noise. Cells that did not produce spikes in response to changes in illumination were not recorded (about 10–40% of approached cells did not spike in response to changes in illumination). Visual stimuli (see below) were cycled, and for the majority of cells every stimulus type was presented eight times in total (8.4 on average). Whole-cell patch-clamp recordings were performed at either −45 or +5 mV holding potentials (not adjusted for junction potential), to isolate excitatory and inhibitory currents, respectively. Signals were measured with a Multiclamp 700B amplifier (Molecular Devices, Union City, CA, USA), digitised at 10 kHz using a Digidata 1440A board (Axon Instruments), and recorded in PCLAMP 10 software. Data were later processed offline, in a set of custom MATLAB functions.

We found that all methods of inducing paralysis worked reasonably well, although about 20% of animals were not completely paralysed after 1 h exposure to 0.1 mM tubocurarine in the recording chamber. We also found that OT neurons chronically exposed to 0.1 mM tubocurarine were on average more spiky than those exposed to 1 μM bungatoroxin in loose-cell-attached experiments (7.5 ± 5.5 spikes/stimulus for tubocurarine, 2.6 ± 3.1 spikes/stimulus for bungarotoxin, n = 37 and 23, N = 8 and 6, respectively, P_{MW} = 8e−6). The proportion of collision-selective cells (as estimated by comparing spiking in response to 'flash' and 'crash' stimuli, Mann–Whitney test with a 0.05 threshold) was not different between experiments with bungarotoxin and tubocurarine (78 and 73%, respectively, P_{MW} = 0.7). The average levels of selectivity for each cell (see 'Statistical methods' below) were also not different

© 2014 Federation of European Neuroscience Societies and John Wiley & Sons Ltd

(n = 37 and 23, N = 8 and 6, respectively, P_{MW} = 0.08). This suggests that the data obtained in experiments performed with bungarotoxin and tubocurarine can be combined together. We also found that different batches of tubocurarine (two batches from Sigma-Aldrich and one batch from Tocris) had markedly different potency in inducing paralysis, and thus the nominal concentrations of tubocurarine may not be indicative of the actual potency of the drug.

The amplitude of recordings from the optic nerve varied greatly across preparations, so we employed a unified adaptive approach to their analysis. The data were first high-pass filtered with a cutoff frequency of f_h = 10 Hz, then taken at their absolute value, and hard thresholded at 3σ, where σ is the noise level (SD) estimated on a segment preceding the stimulus. For cumulative amplitude comparison, the integral of this signal over time was calculated across 2 s after the stimulus. We assumed that the value of this integral reflected the total number of spikes sent through the optic nerve during the response. To estimate the response latency we found the point at which the integral over time exceeded 10% of its final value.

In experiments with pharmacological modulation of network activity we used three modified ACSF compositions: (i) with $[K^+]_{out}$ increased from 4 to 6–7 mM (through the addition of KCl); (ii) with 0.1 mM of picrotoxin; and (iii) with 5 μM of diazepam. Bungarotoxin and one batch of tubocurarine were obtained from Tocris; all other chemicals were obtained from Sigma.

Visual stimulation

The visual stimulation device was custom built by H.X., and consisted of a miniature LCD screen (Kopin Corporation, Taunton, MA, USA), back-lit with a powerful light emission diode [either red (LXHL-LD3C), wavelength 645 nm, or blue (LXHL-LB3C), wavelength 490 nm; Lumileds Lighting, USA; both colors are highly visible for *Xenopus* tadpoles (Parker *et al.*, 2010; Blackiston & Levin, 2012)], and projected by a lens onto one end of a high-fidelity image fiber (600 μm in diameter) (Fujikura Ltd, Tokyo, Japan). The other end of the fiber was brought to the tadpole's eye, placed at 400–600 μm from the lens of the eye, and centered along the eye axis, covering about 60–100° of the visual field. The fiber consisted of 3e+4 image elements, but the stimulus resolution was limited by that of the LCD screen, with 120 pixels across the diameter of the projection field.

In a separate set of experiments we assessed tadpole visual acuity by projecting checkerboard patterns of different tile sizes on the fiber, and inverting this pattern periodically, while recording the spiking output in the OT. In these experiments, with the checkerboard tile angular size fixed at 20–40°, the OT cells responded best (with about 80% probability) when the fiber was placed at 500 μm or further from the lens [consistent with Richards *et al.* (2012)]. The response probability fell below 50% as the fiber was brought closer than 300 μm from the lens (n = 4 cells, N = 3, total of 893 presentations). As we desired the fiber surface to cover at least 60° of the visual field, which was only possible when the fiber was placed at 530 μm from the lens or closer, we used a trade-off distance of 400–600 μm between the fiber and the eye. At these distances the threshold of 50% in response probability was observed for a tile angular size of 8°.

Visual stimuli (see Video S3) were generated in Matlab using the Psychophysics toolbox, and included (Fig. 3B): (i) instantaneous change in luminance from light to darkness ('flash'); (ii) gradual change in luminance from light to darkness ('ramp'), with light intensity following the rule of $c = 1 - t^2$; (iii) simultaneous linear expansion of 25 black squares (5 × 5 grid) over the course of 1 s ('grid'); (iv) a dark circle linearly expanding from the center of the screen ('crash'), with radius changing as $r = R \cdot t$, where R denotes fiber radius in pixels; and (v) 'control', or no stimulus (only used in behavioral experiments with partially immobilised tadpoles). Stimuli were delivered every 20 s and each of the stimuli was 1 s long; the screen was kept dark for 4 s after the end of the stimulus, and then blanked. We used dark stimuli on a light background, as in a pilot set of experiments we observed that OT cells spiked more in response to dark stimuli on a light background (7.1 ± 5.4 spikes/stimulus) than to identical light stimuli on a dark background (2.7 ± 3.4 spikes/stimulus, n = 34, N = 7, P_W = 2e−13), confirming earlier observations that the OT mostly receives inputs from dimming detectors in the retina (Lettvin *et al.*, 1959; Ingle & Hoff, 1990; Waldeck & Gruberg, 1995; King *et al.*, 1999; Ishikane *et al.*, 2005; Nakagawa & Hongjian, 2010; Shen *et al.*, 2011). Note that our linearly expanding stimulus was slower than a realistic collision, as for a realistic collision r would be inversely proportional to the time to collision: $r = k/(t - t_0)$. It is known that frogs exhibit avoidance from linearly expanding visual stimuli (Ishikane *et al.*, 2005), and by using linear expansion we aimed to isolate selectivity to stimulus geometry from selectivity to rapidly accelerating stimuli, which can be mediated by different mechanisms (Peron & Gabbiani, 2009a; Nakagawa & Hongjian, 2010).

Statistical methods

As most of the data reported in this study were markedly non-normal, and had frequent outliers, we preferred non-parametric tests to parametric tests. For all non-paired comparisons across groups we used the Mann–Whitney test (P_{MW}), not adjusted for multiple comparisons. For paired data we report the results of a Wilcoxon signed-rank test (P_W). When multiple comparisons were involved, we report whether the difference was significant after either Bonferroni, or false discovery rate correction (Benjamini & Hochberg, 1995), depending on which correction was more suitable for the context. For multivariate grouped data, results of the ANOVA test (P_{ANOVA}) are reported. For correlations we show P-values of the Student's t-test against the hypothesis of no correlation (P_{Corr}), as well as the Pearson coefficient r. The effect size, when reported, is defined as $E_{12} = (m_1 - m_2)/\sqrt{(\sigma_1^2 + \sigma_2^2)/2}$, where $m_{1,2}$ are the mean values, and $\sigma_{1,2}$ are the trial-to-trial SDs of responses (Hentschke & Stuttgen, 2011). To quantify the selectivity of individual cells, we computed F statistics in the same way as defined for ANOVA calculations: $F = \frac{\text{variance between stimulus types}}{\text{variance within stimulus types}}$. The resulting value depended on both the differences between mean responses to different stimuli, and individual response variability. For this subset of data, sample sizes were very consistent across groups, and for a few cells in which the number of presentations per stimulus type was higher, we bootstrapped the data by randomly downsampling it 50 times at a proper n (8), and then averaged the F-values.

Results

Stimulus selectivity in freely-swimming tadpoles

To provide proper context to the electrophysiological experiments we first systematically described collision avoidance behavior in freely-swimming *Xenopus* tadpoles. Freely-swimming animals were presented with a computer-generated black circle that was projected on the floor of a round experimental chamber, and that approached them at collision, or near-collision trajectories (Fig. 2A; see Video S1, and Materials and methods for details). We recorded 881 collisions from 76 animals, across 15 different speed and size combina-

© 2014 Federation of European Neuroscience Societies and John Wiley & Sons Ltd

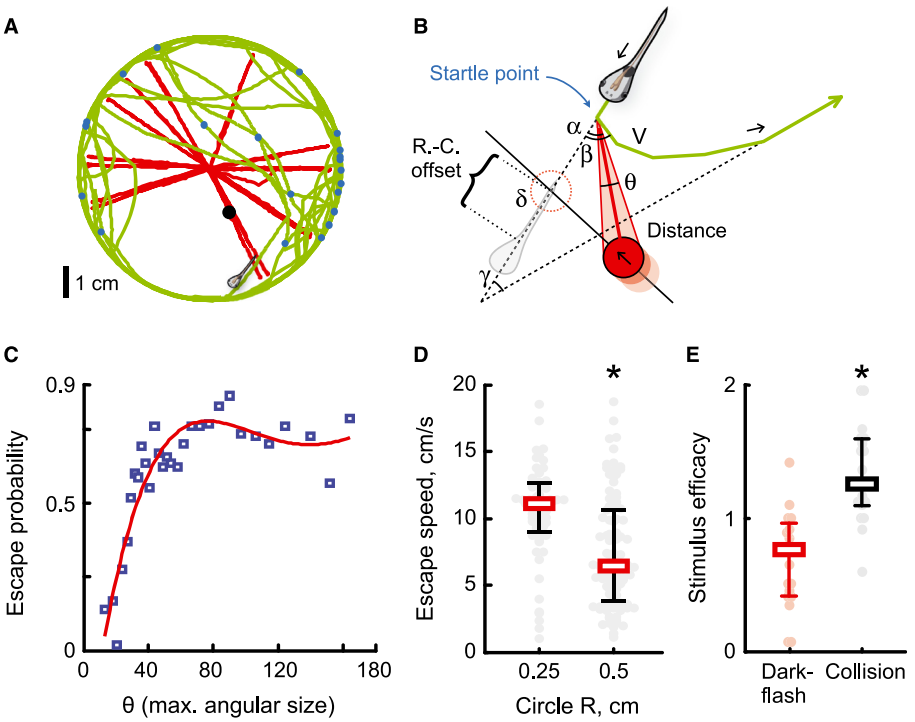

FIG. 2. Behavioral experiments in freely-swimming tadpoles. (A) Trajectories of the tadpole and the visual stimulus over the course of one experiment; small dots represent points of avoidance maneuver initiation. Scaled images of a circle and a tadpole are superimposed on their respective trajectories. (B) A summary of the parameters measured for every collision (see Materials and methods for a detailed description; R.-C. offset stands for rostro-caudal offset). (C) Escape probability as a function of visual stimulus maximal angular size during the collision event; each square represents an average of 29 events and the red line is a fourth degree polynomial fit. (D) One of the pair-wise comparisons between escapes in response to stimuli of different size. Gray circles represent data from individual collision events, boxes and whiskers show medians and interquartile ranges, and the asterisk marks statistical significance ($P < 0.05$). Tadpoles escaped from smaller circles at a faster speed than from larger ones. (E) Relative efficacy (probability of triggering an avoidance maneuver, normalised over the individual responsiveness of each animal), as observed in freely-swimming tadpoles, for dark circles either colliding with the animal, or instantaneously appearing near it.

tions of the approaching object. After the trajectories of both the tadpole and the circle were tracked, we reconstructed the geometry of each collision and each escape maneuver. A diagrammatic summary of the variables measured is shown in Fig. 2B.

Overall, escapes were triggered in 60% of collisions. An average escape maneuver was initiated at a distance of 0.9 ± 0.4 cm from the circle, when the angular size of the circle for the tadpole (θ) reached 45 ± 21°. The tadpole performed a turn, changing its swimming direction at an average angle of β = 84 ± 21°, and rapidly accelerated from a baseline of 1.3 ± 1.0 to 9.9 ± 4.2 cm/s, reaching maximum speed at 133 ± 67 ms after the turn (median and interquartile range). The probability of triggering an escape did not change as the speed of the circle varied (from $v_c = 0$, for avoidance of stationary circles, to 5.8 cm/s, with circle size fixed at $r_c = 0.28$ cm; $P_{ANOVA} = 0.8$; $N = 32$), and neither did it change if the circle size varied (from $r_c = 0.15$ to 0.56 cm; with circle speed fixed at $v_c = 2.9$ cm/s; $P_{ANOVA} = 0.1$; $N = 39$).

Although the escape probability did not depend on the size and speed of the circle, it did depend on the trajectory at which the circle approached the tadpole. To classify trajectories by their geometry we registered movements of both the tadpole and the circle during initial approach, and linearly extrapolated them beyond the moment of escape. We measured the values of predicted minimal distance between the center of the circle and the tadpole, and the angular size of the circle (θ_{max}) from the animal's 'point of view' at the moment of extrapolated closest encounter (Fig. 2B; see Materials and methods). When all collisions were sorted by the approaching circle's angular size θ, and binned in bins of equal sample size (29 collisions per bin) an increase in escape probability as a function of θ became obvious (Fig. 2C). The escape probability exceeded 50% at the threshold angular size of 34°; in contrast, the maximal relative angular expansion rate $(\theta'/\theta)_{max}$, also known as the inverse time-to-collision parameter (Keil & Lopez-Moliner, 2012), was not a good predictor of escape probability.

To check whether any other parameters of collision events were important for triggering an escape, we compared different measurements of collisions in which the escape behavior was triggered ('successes') with those that were ignored ('failures'). The 'successful' and 'failed' collision trajectories did not differ in the rostrocaudal position along the animal axis at which the approaching circle was targeting (rostrocaudal offset value, $P_{MW} = 0.2$), absolute tadpole speed before the collision ($P_{MW} = 0.3$), or direction towards the dot relative to the direction of swimming (α) at the moment immediately before the expected escape ($P_{MW} = 0.9$). We concluded that the angular size of the approaching object θ was the main collision parameter that triggered the escape response.

We then investigated whether the geometry of avoidance maneuvers was influenced by the geometry of the collisions that triggered them. We found that, when all maneuvers were considered, there was no correlation ($P_{Corr} > 0.05$, $n = 533$) between the resulting turn angle (β) and the circle speed, circle size, circle angular size θ, direction to the circle (α), angle between the trajectories (δ), or ro-

© 2014 Federation of European Neuroscience Societies and John Wiley & Sons Ltd

strocaudal position of the point towards which the circle approached (rostrocaudal offset). An absence of correlation between the offset value and turn angle (β) means, in particular, that, although tadpoles escaped in a broad range of directions (β = 84 ± 21°), they did not preferentially escape forward (accelerating) when the circle chased them from behind, or targeted the tail. Similarly, tadpoles did not have a tendency for reversing swimming direction when circles approached them frontally, or targeted their head. Avoidance maneuvers seemed to be performed in a random direction regardless of the collision geometry. Note, however, that we did not assess the laterality of escapes (Wassersug *et al.*, 1999; Wassersug & Yamashita, 2002), as tadpoles tended to swim along the sides of the container (Blackiston & Levin, 2013), and therefore the majority of avoidance responses also happened near the container side, which obviously constrained escape trajectories to one-half of all possible directions (Fig. 2A). The temporal and spatial resolution of our recordings was not fine enough to assess the dynamics of interaction with the barrier during avoidance initiation.

The escape speed also did not vary across the majority of circle speed/size combinations tested (with r_c fixed at 0.28 cm and v_c changed: r_{corr} = 0.12, P_{Corr} = 0.1, n = 217, N = 32; with v_c fixed at 2.9 cm/s and r_c changed: r_{corr} = 0.08, P_{Corr} = 0.2, n = 223, N = 34). When we looked at pair-wise comparisons between escapes from circles of different size and speed, however, we found two distinct threshold-like transitions in escape velocity on the very edges of the sampled range of collision parameters (these differences in escape velocity were significant after Bonferroni correction for multiple comparisons, total of 105 pair-wise comparisons, Mann–Whitney test). For fast-moving circles (speed fixed at v_c = 2.9 cm/s), tadpoles escaped from the medium-sized circles (r_c = 0.28 cm; n = 91, N = 11) faster than from the smallest circles (r_c = 0.13–0.19 cm; n = 34, N = 8 animals; escape speed = 11.6 ± 3.9 and 8.3 ± 3.0 cm/s, respectively, P_{MW} = 3e−5). For slow-moving circles (v_c = 1.4 cm/s), the effect had an opposite sign, i.e. tadpoles escaped faster from smaller circles (r_c = 0.28 cm; escape speed = 10.4 ± 3.5 cm/s) than from larger circles (Fig. 2D; r_c = 0.56 cm; escape speed = 7.4 ± 4.2 cm/s; P_{MW} = 1.8e−0.06, n = 59 and 94, N = 8 and 10, respectively). We found that the turn angle correlated with the escape velocity (r = 0.26; P_{Corr} = 7e−10), with faster escapes preceded by sharper turns [as in classic fast C-starts (Korn & Faber, 2005; Preuss *et al.*, 2006; Burgess & Granato, 2007)], and slower escapes accompanied by just a slight correction of the swimming direction [as in S-starts in fish (Domenici & Blake, 1997)]. We can therefore hypothesise that tadpoles not only either escaped from the stimulus, or ignored it, but also implemented at least two different motor programs, depending on the dynamics of the collision. (See Video S2 for an example of a 'slow' escape maneuver, as opposed to a 'fast' escape maneuver in Video S1).

As the escape maneuver probability appeared to depend only on the final angular size of the object, we decided to check whether the very fact of a dynamic collision with a circle was important for triggering an escape, or whether it was only necessary for an object large enough to appear in the tadpole's visual field to trigger a response. To test this, we performed a series of experiments in which a circle (r_c = 0.28 cm) either approached a tadpole as described above (at a speed of v_c = 2.9 cm/s), or instantaneously appeared near a tadpole. In these experiments 'collisions' triggered escapes in 60% of cases (64 out of 107; 19 animals), whereas instant 'flashes' triggered escapes in only 34% of cases (33 out of 97, N = 19; P_W = 6e−5). We therefore concluded that the tadpole brain is selective for 'collision', or 'looming' stimuli, and that these stimuli are more salient in triggering escape behaviors than the instantaneous 'dark flashes' (so-called because they consist of a black circle on a white background, Fig. 2E).

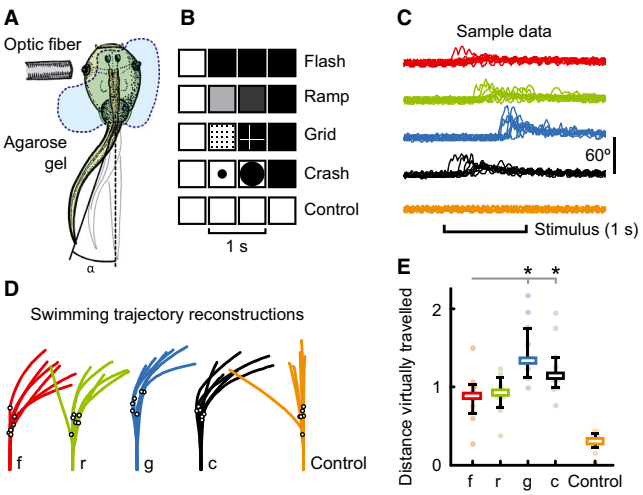

FIG. 3. Experiments in partially immobilised animals. (A) General view of the preparation, with the animal partially immersed in agarose gel, and an optic fiber placed near the eye. (B) Simplified representation of stimuli presented to the animal. Here 'flash' or 'f' represents an abrupt change in lightness, 'ramp' or 'r' represents a gradual change, 'grid' or 'g' stands for an array of linearly expanding squares, 'crash' or 'c' stands for a linearly expanding circle, and 'control' stands for the absence of a visual stimulus. (C) Typical responses (tail deflections) to these stimuli. (D) Sample swimming trajectory reconstructions for different stimuli; black circles mark the response onset. (E) Average 'distances virtually traveled' for every animal, in response to different stimuli (see Materials and methods); boxes represent medians, black whiskers show the interquartile range, and gray lines and asterisks indicate comparisons with 'flash' with P_W < 0.05.

Partially immobilised behavior preserves looming selectivity

As electrophysiological recordings in freely-swimming tadpoles are problematic, we aimed to design a reduced preparation in which the animal would be able to behave, yet remain immobilised. We used a miniature projecting device, equipped with an optical fiber bundle, to bring a computer-generated image to the eye of an intact tadpole. To confirm that visual stimuli delivered in this way can trigger escape behaviors, in the first set of experiments we partially immobilised tadpoles by embedding them in a low-melt agarose gel, leaving one eye and the tail free (Fig. 3A, also see Materials and methods). We then recorded movements of the tail as visual stimuli were delivered (see Video S3), tracked the position of the tail tip over time, and reconstructed swimming trajectories that the animal supposedly tried to implement.

As our goal was to understand the mechanisms underlying the detection of looming stimuli, we designed a set of stimuli aimed at dissecting the information-processing steps in the brain by gradually stripping a typical looming stimulus of its characteristic features (Fig. 3B; Video S4). The first stimulus in the set, which was dubbed 'crash', mimicked a collision, and presented a black circle expanding from the center of the screen over the course of 1 s, to eventually cover the whole surface of the fiber. A stimulus (dubbed 'grid') presented a grid of squares that were planted across the receptive field, and expanded synchronously; this stimulus did not have the global geometry of an actual collision, but preserved the local 'expansion' feature at every part of the retina. A whole-field brightness ramp (dubbed 'ramp') did not have any spatial features of a looming

© 2014 Federation of European Neuroscience Societies and John Wiley & Sons Ltd

stimulus, but preserved the temporal pattern of average luminance change. Finally, the simplest stimulus had neither a spatial nor temporal pattern to it, and presented an instantaneous change in brightness (dark flash, dubbed 'flash'). All stimuli except 'flash' followed the same temporal evolution of brightness. We also introduced a 'control' condition in which no visual stimulus was presented at all.

We recorded 415 responses from 11 tadpoles (a set of typical motor responses to visual stimuli is shown in Fig. 3C). We found that all stimuli successfully triggered escape responses compared with control ($P_W < 9e{-}3$, $N = 11$), with probabilities ranging from 60% (for 'ramp') to 87% (for 'grid'). Differences in response probabilities were not significant across stimuli ($P_W > 0.5$ after Bonferroni correction), but the latencies were different ($P_{ANOVA} = 1e{-}6$), and ranged from 518 ± 226 ms for 'flash' to 982 ± 103 ms for 'grid'. We then performed spectral analysis of the responses, looking separately at the low-frequency band (0–5 Hz, corresponding to slow deflections of the tail, which were probably equivalent to 'turns' in a freely-swimming animal), and high-frequency band (12–40 Hz, corresponding to increases in tail oscillation frequency, or intended swimming acceleration). When all responses across all animals were compared, the low-frequency component (tail deflections, or 'virtual turns') was different from control for all stimuli ($P_{MW} < 6e{-}7$; $N = 11$, $n = 66, 75, 67, 67,$ and 75; relative low-frequency contribution = 23 ± 24%, 37 ± 23%, 34 ± 22%, 37 ± 22%, and 39 ± 23% for control, 'flash', 'ramp', 'grid' and 'crash', respectively), whereas the high-frequency component (or 'virtual acceleration') was different from control for all stimuli except 'flash' ($P_{MW} < 0.02$; $N = 11$, $n = 66, 75, 67, 67,$ and 75; relative high-frequency contribution = 2.8 ± 3.0%, 2.6 ± 4.2%, 3.1 ± 5.8%, 6.9 ± 11.0%, and 5.7 ± 9.7% for control, 'flash', 'ramp', 'grid' and 'crash', respectively). The responses to 'grid' and 'crash' had a higher spectral power in the high-frequency band than the responses to 'flash' ($P_{MW} < 0.02$), suggesting that, compared with a simpler 'dark flash', more realistic collision stimuli triggered faster 'virtual avoidance maneuvers', with sharper 'virtual turns', similar to how different stimuli evoked different types of avoidance maneuvers in freely-swimming animals. All differences reported here were significant after a false discovery rate correction for multiple comparisons.

To better compare responses to different stimuli, taking into account not only the presence of a response, but also its dynamics and spectral content at both frequency bands, we aimed to approximately reconstruct the swimming trajectories that tadpoles attempted to implement when reacting to the stimuli (Fig. 3D). Having only one point of the tail tracked, we could not build a realistic kinematic model of the animal, and followed a simplified approach. We assumed that an increase in the tail oscillation frequency would normally make the tadpole move faster, whereas slow lateral tail deflections would make it turn, and in a simple model estimated the distance that the tadpole would have traveled during the escape response, compared with 'baseline swimming' (see Materials and methods). These uncalibrated 'average distances virtually traveled' were longer than control for all stimuli ($P_W < 0.012$; Fig. 3E), and the 'virtual distances traveled' in response to 'crash' and 'grid' stimuli were longer than for 'flash' ('crash': 10 tadpoles out of 11, $P_W = 0.01$; 'grid': 9 tadpoles out of 10, $P_W = 0.02$). We concluded that, first, visual stimuli provided by our projecting device were effective in simulating collisions and eliciting escape behaviors, and, second, the difference in saliency between the looming stimulus ('crash') and the full-field 'flash' was preserved in this preparation. This made it possible for us to move to the next step of the study, and to perform electrophysiological recordings of neural activity underlying the avoidance response.

Electrophysiological responses to behaviorally-salient stimuli

As described in the Introduction, the shortest feed-forward circuit connecting primary afferents in the tadpole retina to the muscles in the tail consists of only five neurons. Moreover, the motor command is likely to be finalised at the level of the fourth neuron in this chain (reticulospinal neurons of the hindbrain) (Perrins *et al.*, 2002; Korn & Faber, 2005; Fetcho & McLean, 2010; Huang *et al.*, 2013). This means that the stimulus selectivity, defined as a preference for the 'crash' stimulus over the 'flash', is likely to arise in the retina (Ishikane *et al.*, 2005; Baranauskas *et al.*, 2012), tectum (Nakagawa & Hongjian, 2010), or hindbrain (Ingle & Hoff, 1990; Preuss *et al.*, 2006). To pinpoint the region in which the looming stimulus selectivity can first be observed as a difference in electrophysiological responses, we recorded four types of signals in the brain: (i) bulk spiking in the optic nerve, (ii) inhibitory and (iii) excitatory synaptic inputs to the OT cells, and (iv) spiking output of OT cells (Fig. 4, see Materials and methods). We then compared the amplitudes of the total cumulative responses across the same set of stimuli that were used in the partially immobilised preparation (Fig. 3).

As the absolute amplitudes of recorded signals were highly variable, and as our data were paired (responses to stimuli of every type were recorded in every cell and animal), in Fig. 4 we present the relative amplitudes, normalised to the average amplitude across all four stimuli for each cell (for synaptic and spiking data) or animal (for optic nerve data). In the optic nerve (Fig. 4A) responses to 'flash' were stronger than to any other stimulus ($P_W < 1e{-}3$, $N = 22$), whereas responses to either 'crash' or 'grid' were relatively weak. Similarly, inhibitory synaptic currents recorded in OT neurons (Fig. 4B) were not selective for looming stimuli, with responses to 'ramp' being marginally lower than those to 'flash' and 'crash' ($P_W < 0.03$, $n = 28$, $N = 5$). In contrast, excitatory synaptic currents in OT neurons (Fig. 4C) exhibited weak selectivity for 'crash' compared with 'flash' ($P_W = 0.02$, $n = 28$, $N = 5$), whereas at the level of OT spiking (Fig. 4D) this selectivity became significant for both 'crash' and 'grid' stimuli ($P_W = 2e{-}6$, $n = 56$, $N = 14$ for both comparisons), such that both stimuli evoked twice as many spikes per stimulus (6.18 ± 5.73 and 6.19 ± 5.72, respectively) than 'flash' (2.99 ± 3.00). 'Crash' produced stronger spiking than 'flash' in 71% of cells, and in 88% of these cells selectivity was statistically significant at the individual cell level ($P_{ANOVA} < 0.05$). In contrast, glutamatergic synaptic inputs were stronger for 'crash' than for 'flash' in only 64% of cells, and in only 44% of these cells was the difference significant ($P_{ANOVA} < 0.05$). This suggests that selectivity for looming stimulus may not fully arise until the level of tectal cell output. The absolute amplitudes for 'flash', 'ramp', 'grid' and 'crash', respectively, were found to be: for inhibitory currents (total charge, in pC): 10.5 ± 11.0, 7.6 ± 9.5, 9.3 ± 8.5, and 10.6 ± 9.1; for excitatory spiking (in pC): −6.4 ± 5.5, −6.2 ± 3.9, −7.5 ± 6.1, and −8.5 ± 4.8; and for OT spiking (*n* spikes): 3.0 ± 3.0, 4.9 ± 4.9, 6.2 ± 5.7, and 6.2 ± 5.7.

It is important to note that one key difference between the optic nerve recordings and the single tectal cell recordings was that in one case we were looking at the bulk activity of several retinal ganglion cells (RGCs), whereas in the other we were looking at selectivity in individual neurons, potentially making them difficult to compare. However, sampling the responses of individual tectal cells from multiple animals is conceptually equivalent to detecting the responses of a large ensemble of cells from one animal, as long as synchrony and variability of responses are not concerned, and sampling is random.

© 2014 Federation of European Neuroscience Societies and John Wiley & Sons Ltd

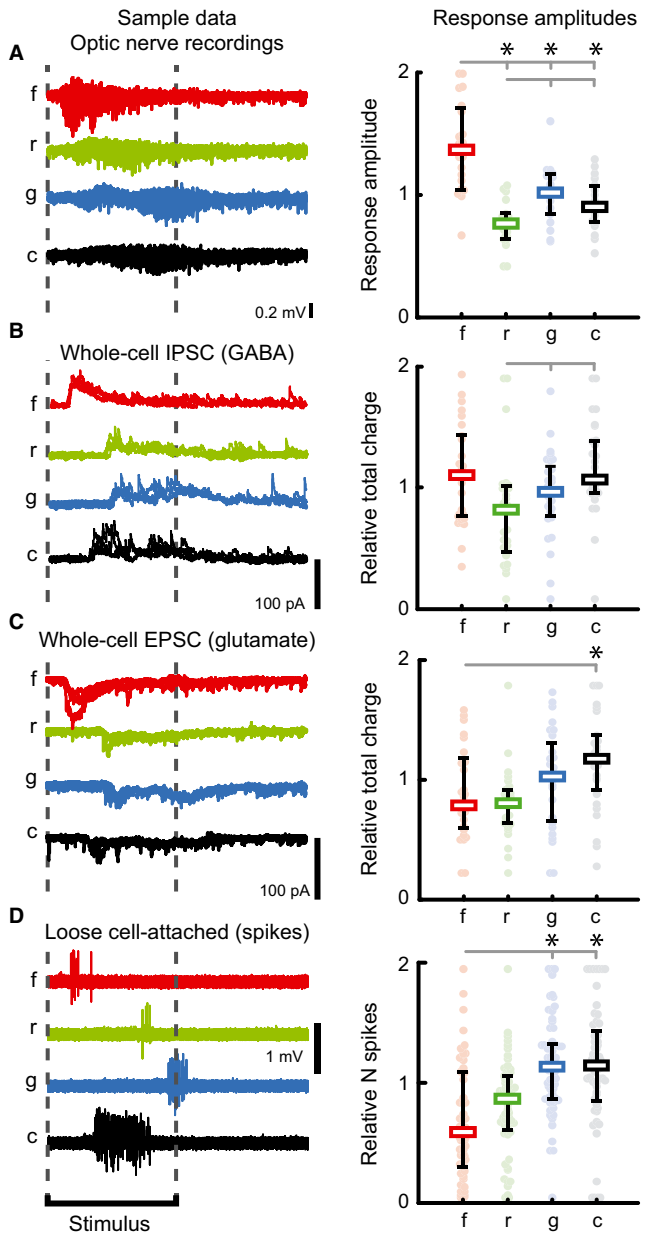

FIG. 4. Typical responses to visual stimuli recorded at different points in the visual system, and their relative cumulative response amplitudes. (A) Recordings from the optic nerve. (B and C) Whole-cell recordings in the OT for inhibitory and excitatory currents, respectively. (D) Spiking output of the OT cells. In every panel 'f' stands for 'flash', 'r' for 'ramp', 'g' for 'grid', and 'c' for 'crash'. For relative response amplitudes (right column) all measurements are shown as gray circles, together with medians represented by boxes, and interquartile ranges. Gray lines and asterisks mark significance levels of $P < 0.05$ compared with response to 'flash'. Outliers were brought into axes limits. EPSC, excitatory post-synaptic current; IPSC, inhibitory post-synaptic current.

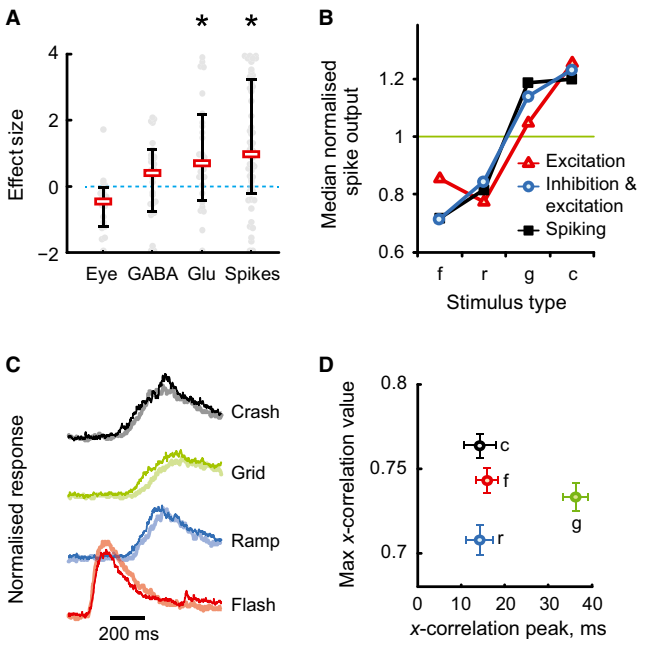

FIG. 5. Role of excitation in inhibition in looming stimulus selectivity. (A) Effect size (difference between responses to 'crash' and 'flash', divided by trial-to-trial variability) observed at different stages of information processing in the tadpole brain. Left to right: recordings in the optic nerve (Eye), GABAergic inputs to OT cells (GABA), glutamatergic inputs to OT cells (Glu), and OT cell spike output (Spikes). Asterisks mark effects that are significantly larger than zero. (B) Predictions of cell spike output that are based on amplitudes of synaptic excitation and inhibition (circles) match actual median normalised spike output (black squares) better than those based on excitatory inputs alone (triangles). Stimuli were normalised by the average response across all stimulus types (similarly to Fig. 4). See details in the text. (C) Average synaptic responses to different visual stimuli, normalised by total synaptic charge, with inhibitory (pale wide line) and inverted excitatory (darker narrow line) curves superimposed. Inhibitory currents are lagging behind excitatory currents for all stimuli. (D) Average positions and values of cross-correlogram peaks for excitatory and inhibitory synaptic currents recorded in OT cells (horizontal axis represents the lag between excitation and inhibition; $n = 28$; whiskers represent SEM). Responses to 'flash' and 'crash' are not significantly different ($P_{MW} > 0.05$). f, 'flash'; r, 'ramp'; g, 'grid; c, 'crash'.

Although multiple cell types are described in the OT of adult *Xenopus* frogs (Lazar & Szekely, 1967; Lazar, 1973) and other species (Grüsser & Grüsser-Cornehls, 1976; Wang & Frost, 1992; Ewert, 1997; Frost & Sun, 2004; Kang & Li, 2010; Nakagawa & Hongjian, 2010; Liu *et al.*, 2011), and in both mammals and birds different cell types in the OT are known to have different dynamics of responses to looming stimuli (Frost & Sun, 2004; Liu *et al.*, 2011), we failed to identify any distinct cell types through our data, despite the high variability of response dynamics in OT cells. This further supported the evidence that, at the developmental stages that we worked with, cell types in the tadpole OT are not yet fully developed.

To compare looming stimulus selectivity across different stages of signal processing we calculated the mean effect size of this selectivity, defined as the difference between average responses to 'crash' and 'flash' divided by the trial-to-trial SD of response amplitudes (Hentschke & Stuttgen, 2011). We found that the effect size gradually increased as the signal progressed through the circuit (Fig. 5A; $P_{ANOVA} = 1e{-}4$): from -0.5 ± 0.8 in the optic nerve (the value was negative due to reversed 'flash/crash' selectivity), through 0.1 ± 1.5 for GABA and 0.9 ± 1.8 for glutamatergic synaptic inputs, to 1.3 ± 2.0 for spiking. We therefore concluded that the OT was the first brain region in which the behavioral saliency of looming stimuli is encoded by population response amplitudes.

Our data, however, did not provide enough evidence about the exact mechanisms of collision detection. We considered two broad models that could explain the looming stimulus selectivity in the OT. One model assumes that looming stimuli are detected at the level of excitatory synaptic inputs to OT cells, and this selectivity is

© 2014 Federation of European Neuroscience Societies and John Wiley & Sons Ltd

further amplified and thresholded by OT cell spiking. Notably, this model implies higher involvement of retinal processing and targeted feed-forward retinotectal projections in the detection of looming stimuli. For example, retinal circuits could implement temporally localised surround inhibition (Lettvin *et al.*, 1959), and report the results of this computation to the OT by some kind of temporal code (Ishikane *et al.*, 1999, 2005; Baranauskas *et al.*, 2012). Alternatively, RGCs from different regions of the retina could use a population code, with a small subset of influential selective 'labeled lines' establishing targeted convergent connections onto a subtype of OT cells (Grüsser & Grüsser-Cornehls, 1976; Ewert, 1997), turning them into 'expansion detectors' (Frost & Sun, 2004). In contrast, another model assumes that looming stimuli are detected through the emergent dynamic activity of the OT network as a whole (Xu *et al.*, 2011), and that stronger synaptic drive during looming stimuli, as was observed in our experiments, is due to recurrent connectivity in the OT (Pratt & Aizenman, 2007; Pratt *et al.*, 2008), and comes as a consequence, rather than a cause of stronger spiking in the tectum. In this model, collision detection relies on distributed computations (Lamme & Roelfsema, 2000), and dynamic activation patterns (Das *et al.*, 1996; Meredith & Ramoa, 1998; Zhu & Lo, 2000; Lee & Hall, 2006) that are dependent on the interplay between direct and recurrent inputs in this network (Tao & Poo, 2005; Richards *et al.*, 2010; House *et al.*, 2011; Shen *et al.*, 2011; Shao *et al.*, 2013).

To differentiate between these 'mostly feed-forward' and 'mostly recurrent' models we first tested whether the total synaptic drive received by each OT cell can serve as a good predictor of its spike output. As the synaptic data (Fig. 4B and C) and spiking data (Fig. 4D) were recorded from different sets of cells, we could not compare the synaptic inputs with the spiking output directly. Instead, we used the synaptic amplitudes of excitatory and inhibitory inputs recorded in a subset of OT cells to 'predict' the probable spiking output of these cells ($n = 28$), and then compared the distribution of 'predicted output amplitudes' with recordings of spiking in another set of OT cells ($n = 56$). We assumed that inhibitory inputs hyperpolarised the membrane, and also decreased the membrane resistance through shunting inhibition (Isaacson & Scanziani, 2011); therefore the predicted spike output of each cell was modeled as $s = c\frac{e-ai}{1+bi} + d$, where e is the relative excitation strength, normalised across stimuli (Fig. 4B), i is the relative strength of inhibition (Fig. 4C), and a, b, c and d are unknown parameters. We optimised these parameters, looking for the best fit between median spiking amplitudes predicted for cells from the first group, and actual spiking recorded from cells from the second group (Fig. 5B). Optimal fit was achieved for $a = 0.04$ and $b = -0.02$, and as synaptic drive strengths were normalised, small values of fit parameters indicated that inhibition had a weaker effect on spiking selectivity than excitation. Overall, in this model excitatory synaptic inputs explained 52% of the difference in spiking responses across stimuli, the introduction of inhibitory inputs accounted for another 34%, whereas 15% of the difference remained unexplained. These results showed that synaptic inhibition was likely to directly contribute to the emergence of selectivity in the OT, with differences in the excitation/inhibition balance during responses to different stimuli being, potentially, one of the important sources of this selectivity.

We then investigated the temporal interactions between the inhibitory and excitatory inputs at each cell (Fig. 5C), and tested whether these interactions could contribute to differences in spiking response to different stimuli (Wehr & Zador, 2003; Wilent & Contreras, 2005; Pecka *et al.*, 2008; Zhou *et al.*, 2010; Shen *et al.*, 2011; Person & Raman, 2012; Royer *et al.*, 2012). We calculated cross-correlations between the average time profiles of excitatory and inhibitory inputs for each stimulus type in each cell, and compared peak cross-correlation values, as well as their positions on the correlogram (Okun & Lampl, 2008) (Fig. 5D). Inhibition lagged behind excitation for all stimuli, and this lag did not differ between responses to 'flash' (16 ± 70 ms) and 'crash' (14 ± 103 ms; $P_W = 0.7$; $n = 28$, $N = 5$). The peak cross-correlation for responses to 'flash' and 'crash' also did not differ (0.74 ± 0.21 for 'flash'; 0.76 ± 0.20 for 'crash', $P_W = 0.26$, $n = 28$, $N = 5$). We concluded that the difference in the temporal profiles of excitation and inhibition did not play an active sculpting role in the emergence of stimulus selectivity in individual OT cells, despite the fact that, in the optic nerve, responses to 'flash' were somewhat shorter than responses to any other stimulus (20–80% rise time of the cumulative response, 476 ± 160, 656 ± 201, 647 ± 157, and 681 ± 173 ms for 'flash', 'ramp', 'grid', and 'crash', respectively, $P_{MW} < 0.002$ for all comparisons with 'flash', $N = 22$).

Pharmacological modulation of stimulus selectivity

To investigate the importance of network activation dynamics for stimulus selectivity we recorded the spike output of OT cells *in vivo*, while pharmacologically modulating either their intrinsic properties (Pratt & Aizenman, 2007), or the balance of excitatory and inhibitory synaptic transmission in the OT (Shen *et al.*, 2011). In one series of experiments we used ACSF with elevated potassium concentrations ($[K^+]_{out} = 7$ mM, compared with 4 mM in control) to increase the resting membrane potential of cells in the brain. The subthreshold depolarisation of neurons promotes spontaneous spiking (Shin *et al.*, 2010) and the spontaneous release of neurotransmitters from presynaptic terminals (Jensen *et al.*, 1994; Shin *et al.*, 2011), but also facilitates the inactivation of voltage-gated Na channels, suppressing burst generation (Pratt & Aizenman, 2007; Remy *et al.*, 2010; Tsuruyama *et al.*, 2013). We found that, in ACSF with elevated $[K^+]_{out}$, bursting was suppressed, and OT cells fired fewer spikes in response to visual stimulation (Fig. 6A; 1.8 ± 1.9 spikes/stimulus averaged across all stimuli types for high $[K^+]_{out}$, compared with 5.2 ± 4.6 spikes/stimulus in control; $n = 26$ and 60, $N = 3$ and 14, respectively, $P_{MW} = 4e{-}5$). Selectivity for looming stimuli was lost, and even reversed, with 81% of recorded cells (21 out of 26; $P_W = 2e{-}3$) having a higher response to 'flash' than to 'crash'. The median selectivity effect size in high $[K^+]_{out}$ ACSF was lower than in control (Fig. 6B; $P_{MW} = 2e{-}4$), and negative, reflecting the reversal of stimulus preference.

To differentiate between the emergent stimulus selectivity of the OT network as a whole, and the amount of tuning that each OT cell exhibited individually (Podgorski *et al.*, 2012), we introduced an index of 'individual cell selectivity', defined as a ratio of between-stimuli to within-stimuli variability of responses, and computed in the same way as F statistics are computed for the ANOVA test (see Materials and methods). Note that for any given cell its selectivity index quantified the presence of tuning across stimuli types in our assay, but not necessarily a preference for the looming stimulus. A high selectivity index corresponded to cells that spiked differently across stimuli, and consistently within each stimulus type, whereas low values corresponded to noisy, non-selective cells. In experiments with high $[K^+]_{out}$, the individual selectivity of OT cells was lower than in control (Fig. 6C; $P_{MW} = 3e{-}3$), reflecting higher background noise levels, and lower dynamic range of spiking output.

To check whether the balance of synaptic excitation and inhibition is important for the emergence of stimulus selectivity we pharmacologically manipulated inhibition, by either blocking $GABA_A$

© 2014 Federation of European Neuroscience Societies and John Wiley & Sons Ltd

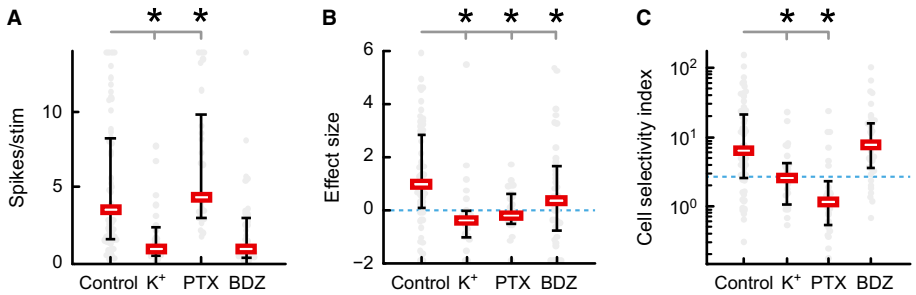

FIG. 6. Pharmacological modulation of OT network activity. In every panel, columns of data represent different experimental conditions [left to right: control experiments, high K^+ ACSF, GABAergic transmission blocked with picrotoxin (PTX), and GABAergic transmission enhanced by diazepam (BDZ)]. Gray circles show individual cell data, red boxes indicate medians, whiskers show interquartile ranges, and gray lines and asterisks indicate significance levels of $P < 0.05$ compared with control; outliers are brought into axes limits. (A) Average number of spikes per stimulus (averaged across all five stimulus types from our assay) generated by OT cells in different solutions. (B) Effect size for OT looming stimulus selectivity (difference between spike outputs in response to 'crash' and 'flash', normalised by response variability); dashed line marks effect reversal. (C) Index of individual selectivity of OT cells (see definition in Materials and methods). Dashed line indicates the value (2.4), which with our sample sizes corresponded to P_{ANOVA} of 0.05 (significance threshold for individual OT cell selectivity, without a false discovery rate adjustment).

receptors with 100 μM of picrotoxin in the external solution, or making inhibition stronger by adding 5 μM of diazepam, a positive modulator of $GABA_A$ receptors (Karayannis *et al.*, 2010; Shen *et al.*, 2011). Unlike many classical preparations, the *Xenopus* OT does not generate rapid epileptiform discharges when inhibition is pharmacologically blocked (Aizenman & Cline, 2007; Pratt & Aizenman, 2007; Pratt *et al.*, 2008; Deeg *et al.*, 2009; Deeg & Aizenman, 2011; Khakhalin & Aizenman, 2012) due to strong inactivation of Na^+ channels in tectal neurons (Pratt & Aizenman, 2007). In solution containing picrotoxin, OT cells became more responsive compared with control (Fig. 6A; 7.1 ± 5.4 spikes/stimulus in picrotoxin vs. 5.2 ± 4.6 in control, $P_{MW} = 0.04$; $n = 25$ and 60, $N = 5$ and 7, respectively). Stimulus selectivity in the OT was, however, completely lost, at both the network level ($P_W = 0.3$; only 40% of cells responded more strongly to 'crash' than to 'flash'), and for every cell individually (only 25% of cells exhibited any individual tuning, based on $P_{ANOVA} < 0.05$ criterion, compared with 70% of cells in control). Respectively, both the OT selectivity effect size (Fig. 6B; $P_{MW} = 6e{-}4$), and the individual cell selectivity index (Fig. 6C; $P_{MW} = 1e{-}5$) were lower in picrotoxin-containing ACSF than in control.

In experiments with GABAergic transmission enhanced by diazepam, global selectivity for looming stimuli was also lost, with the effect size being lower than in control (Fig. 6B; $P_{MW} = 0.047$), as across all cells 'crash' produced a stronger response than 'flash' only at a chance level (in 55% of cells; $P_W = 0.6$, $n = 38$, $N = 5$). At the same time, unlike in experiments with inhibition blocked, most cells remained highly selective individually, and the cell selectivity index was not different from control (Fig. 6C, $P > 0.05$). With diazepam in the ACSF, 79% of cells exhibited statistically significant individual tuning across stimuli (based on the $P_{ANOVA} < 0.05$ criterion; median $P_{ANOVA} = 6e{-}5$), but unlike in the control series of experiments, this individual selectivity was not consistent across the OT, meaning that cells were not necessarily selective for 'crash' stimuli. The average spiking output was lower in experiments with diazepam than in control (Fig. 6A; 2.2 ± 3.0 spikes/stimulus, $P_{MW} = 4e{-}5$).

Could retinal processing account for stimulus selectivity?

Although our data indicated that collision detection can be performed by recurrent networks in the OT, there is still a possibility that detection happened in the retina, and was communicated to the OT via the optic nerve. Although the cumulative amplitudes of optic nerve responses were not selective for looming stimuli, RGCs could detect collisions (Munch *et al.*, 2009; Zhang *et al.*, 2012) and communicate them to the OT by either population code, using a small subset of 'labeled lines' (Frost & Sun, 2004), or by a rate code, with some spiking patterns providing stronger synaptic activation of OT cells than the others (Kuras *et al.*, 2006). In adult ranid frogs, interconnected dimming detectors in the retina (Lettvin *et al.*, 1959; Waldeck & Gruberg, 1995; King *et al.*, 1999) can detect looming stimuli and communicate this information to the OT by switching from desynchronised spiking to globally synchronised oscillations in the 10–30 Hz frequency range (Ishikane *et al.*, 2005; Baranauskas *et al.*, 2012). Oscillations in the 40–60 Hz range were also reported in retinorecipient layers of the superior colliculus in mammals (Brecht *et al.*, 2001; Stitt *et al.*, 2013) and the OT in birds (Goddard *et al.*, 2012). To check whether this effect was present in our preparation we looked at the spectral content of responses in the optic nerve. We found that oscillations in the 10–50 Hz frequency band were prominent in responses to 'flash' (Fig. 7A), with 10 animals out of 22 having an isolated frequency peak within the 10–50 Hz band. This peak was, however, absent from individual spectra of responses to both 'grid' (one animal out of 22 with an isolated frequency peak) and 'crash' (no animals with a peak out of a total of

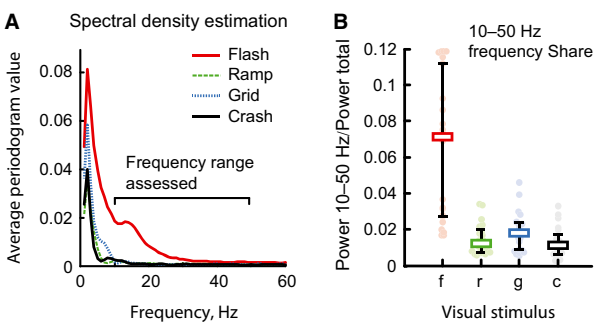

FIG. 7. Temporal coding in the retina does not contribute to the looming stimulus selectivity in the tectum. (A) Average periodograms of optic nerve responses to different visual stimuli. The 10–30 Hz frequency band was prominent in responses to 'flash', but was absent from spectra of responses to both 'grid' and 'crash'. (B) Relative spectral power of the γ-band in responses to different stimuli; the γ-band is more prominent in responses to 'flash' than to all other stimuli ($P_W < 2e{-}5$; $N = 22$). f, 'flash'; r, 'ramp'; g, 'grid'; c, 'crash'.

© 2014 Federation of European Neuroscience Societies and John Wiley & Sons Ltd

22). The relative spectral power of this high-frequency band was more prominent in responses to 'flash', than in responses to all other stimuli (Fig. 7B; $P_W < 2e{-}5$; $N = 22$). We concluded that the synchronised oscillatory spiking of dimming receptors does indeed occur in *Xenopus* tadpoles, but it cannot serve as a mechanism for collision detection at the developmental stages that we studied, as in our assay it was only present in the least salient stimulus, but not in more salient looming stimuli.

Conceptual model

Our data suggested that stimulus selectivity may arise as a result of recurrent connections within the tectum, but is a distributed network of recurrently interconnected cells sufficient to act as a collision detector? To investigate this, we created a simple conceptual model that performed exactly this type of computation. Consider a one-dimensional 'retina' comprised of OFF elements that project to a one-dimensional 'tectum' in a retinotopic fashion. A simple way to visualise the dynamic behavior of a one-dimensional system like that is to plot the evolution of its activation states in consecutive horizontal lines, as is done for cellular automata (Mitchell, 1996; Vladimirov *et al.*, 2012) (Fig. 8). Let us assume that the model follows three simple rules. (i) Every tectal cell receives excitatory inputs from a corresponding cell in the retina, and also recurrent inputs from four cells surrounding it (two at each side), reflecting activation from the previous time step. (ii) Tectal cells spike when the total activation they receive at some time step exceeds a threshold. (iii) After spiking, each tectal cell enters a refractory period for two time steps before it can spike again.

It is straightforward to see that this simple model is tuned to be selective, among other things, to one-dimensional 'looming stimuli' (Fig. 8C), as they produce a higher cumulative output in this system compared with an instantaneous 'flash' (Fig. 8A), receding (Fig. 8B) or translational (not shown) stimuli. The mechanism behind this selectivity is that an expanding stimulus creates a secondary delayed wave of activation in the middle of the 'tectum'; as cells in the middle emerge from the refractory period, they are recurrently excited for the second time by expanding waves of activity around them. Due to simple spatial logic, this 'focus' of secondary excitation does not occur for synchronous or translational stimuli, whereas for receding stimuli recurrent excitation overlaps temporally and spatially with direct excitation from the retina, and so does not produce additional spiking. This model is not the only way to build a distributed looming detector, but it shows that the requirements for such a system are quite low. The ultimate way to check whether distributed processing of this kind happens in the real OT is to perform Ca^{2+} imaging experiments, registering the dynamics of network activity, which will be our next goal.

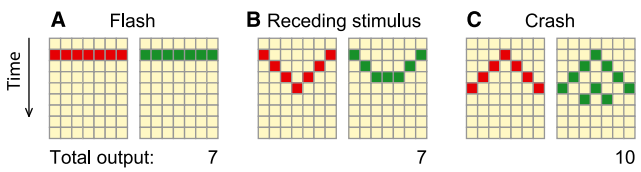

FIG. 8. Conceptual model of a reverberation network acting as a collision detector (see Discussion for details). In every panel the left grid represents a one-dimensional 'retina', and the right grid represents a one-dimensional 'tectum'; rows correspond to discrete time steps (time running from top to bottom), and columns correspond to 'RGCs', or retinotopically arranged 'tectal cells', accordingly. Cells that spike during the current time frame are shown as dark and silent cells are pale. (A) Response to instantaneous 'flash'. (B) Response to reversed looming, or receding stimulus. (C) Response to looming stimulus, or 'crash'. Total cumulative spiking output in the 'tectum' is stronger for 'crash' (10 spikes) than for either 'flash' or receding stimulus (seven spikes each).

Discussion

In this study we present two models for the emergence of selectivity in the OT: one relying on retinal processing (Ishikane *et al.*, 2005; Munch *et al.*, 2009; Zhang *et al.*, 2012) and targeted feed-forward retinotectal connections (Frost & Sun, 2004; Baranauskas *et al.*, 2012), and the other, relying on the recurrent network dynamics in the OT. We suggest that the recurrent model seems to better explain the phenomena described in this study. Because of the fact that, during the developmental stages that we studied, the vast majority of RGC axons in *Xenopus* project to the OT (Steedman *et al.*, 1979; Deeg *et al.*, 2009; Hiramoto & Cline, 2009), and not to other brain regions, we were able to conclude from our optic nerve recordings (Fig. 4A) that the majority of RGCs in the retina did not transmit the results of collision detection by a simple rate code (via the total number of spikes sent). In addition, the absence of synchronised oscillations in response to 'crash' (Fig. 7) makes the use of temporal coding unlikely. It is well established that most, if not all, cells in deep layers of the *Xenopus* OT receive strong direct inputs from the retina (Deeg *et al.*, 2009; Xu *et al.*, 2011), and in this light the fact that in our study the majority (~70%) of OT cells responded to 'crash' more strongly than to 'flash' tentatively argues against the theory of 'dedicated labeled lines' from the retina converging on few specialised collision detectors in the OT in a sparse 'mosaic' manner (Frost & Sun, 2004). We also did not observe any distinct subtypes of OT cells, based on the dynamics of their responses to looming stimuli, as described previously (Frost & Sun, 2004; Liu *et al.*, 2011). We therefore conclude that although an alternative, 'mostly-feed-forward' explanation of our data is possible, and some 'labeled lines' reporting collision events from the retina to the OT may still have been missed by our methods, this alternative explanation may require more elaborate assumptions about the architecture of targeted connections between the retina and the OT, as well as within the OT, and in the absence of decisive evidence in its favor we support a simpler explanation.

The analysis of the excitation and inhibition dynamics shows that the average profiles of excitatory and inhibitory synaptic inputs to OT cells were highly and similarly correlated during responses to both salient and non-salient sensory stimuli. This finding adds to previously described cases of high temporal correlation between synaptic excitation and inhibition in local networks (Wehr & Zador, 2003; Isaacson & Scanziani, 2011), and shows that temporal lags between excitatory and inhibitory inputs to OT neurons were not likely to actively 'sculpt' their spike output (Okun & Lampl, 2008), as happens in some systems (Wilent & Contreras, 2005; Zhou *et al.*, 2010). At the same time, inhibition sharpened selectivity for sensory stimuli in individual OT cells, similarly to known models of narrowly tuned excitation combined with broadly tuned inhibition (Foeller *et al.*, 2005; Wu *et al.*, 2008; Sun *et al.*, 2010; Zhang *et al.*, 2011). Most importantly, however, our pharmacological experiments suggest that local inhibition may maintain optimal levels of recurrent activity in the OT (Shao *et al.*, 2013), regulating the relative strengths of direct and recurrent inputs to OT cells, and allowing for comparison between newly arriving sensory information and traces from the past (Lamme & Roelfsema, 2000). Inhibitory blockade rendered the OT non-selective, and unlike many mammalian preparations, this was not due to spontaneous epileptiform discharges

© 2014 Federation of European Neuroscience Societies and John Wiley & Sons Ltd

disrupting normal functioning (Isaacson & Scanziani, 2011), but rather due to existing recurrent activity in the OT circuits overwhelming direct inputs from the RGCs (Richards *et al.*, 2010). The importance of optimal integration between direct and recurrent inputs was further confirmed in experiments with enhanced inhibition, in which OT cells were prevented from communicating with each other effectively. This disruption of network dynamics rendered the OT non-selective, despite individual cells exhibiting high, but uncoordinated tuning to sensory stimuli.

Similarly, when the intrinsic excitability of OT neurons, and their ability to spike repeatedly, were decreased by K^+-induced membrane depolarisation and related Na^+ channel inactivation, the recurrent network activation in the OT was abolished, and the network was rendered non-selective. These results also provide a perspective on a previous finding that persistent visual stimulation, which makes neurons in the tadpole OT more excitable (Aizenman *et al.*, 2003), partially disrupts visually evoked behaviors (Dong *et al.*, 2009).

Our comparison of the tectal responses to different visual stimuli suggests that the slower a stimulus developed, the higher the total number of spikes that it evoked in the OT. This observation is in seeming contradiction to the fact that quasi-stationary stimuli do not typically produce robust behavioral responses in animals. In the locust, for example, the main function of the collision-detecting neuron appears to be in selecting stimuli that unroll fast enough to overcome the spike-frequency adaptation that the neuron exhibits (Peron & Gabbiani, 2009a,b; Simmons *et al.*, 2013). In the tadpole, however, OT cells do not feed directly to motor neurons, but are connected to reticulospinal neurons in the hindbrain (Szepsenwol, 1935), which are known to perform active temporal thresholding of inputs converging on them (Fetcho, 1991; Preuss *et al.*, 2006). Although the exact electrophysiology of the major reticulospinal neurons in *Xenopus* tadpoles is not yet known, in fish this temporal thresholding is mediated by a competition between excitation and feed-forward shunting inhibition (Fetcho, 1991; Korn & Faber, 2005; Medan & Preuss, 2011). We can therefore assume that, in the tadpole, stimuli that are 'too fast' and 'too slow' may be rejected by two different networks, in the OT and hindbrain, respectively. Moreover, in behavioral experiments we observed two distinct behavioral programs for visually evoked escapes: one with a drastic change in swimming direction and rapid acceleration, and another with a modest increase in the swimming speed, and a slight correction of course. These programs seem to correspond, respectively, to C-starts (Fetcho, 1991; Korn & Faber, 2005), and slow starts (Burgess & Granato, 2007; Portugues & Engert, 2009), or S-starts (Domenici & Blake, 1997), as described in fish (Budick & O'Malley, 2000). The fact that collision events with different dynamics can trigger different motor programs may mean that individual command neurons may be tuned to different dynamics of inputs from the OT, as was suggested previously for hindbrain neurons in fish (Gahtan *et al.*, 2002; Preuss & Faber, 2003; Korn & Faber, 2005; Kohashi & Oda, 2008; Orger *et al.*, 2008; Portugues & Engert, 2009; Whitaker *et al.*, 2011), ranid tadpoles (Ingle & Hoff, 1990), and giant neurons in insects (Card, 2012).

To sum up, here we show that recurrent excitatory and inhibitory connections in the OT, as well as signal integration in individual tectal cells, play a crucial role in the detection of looming stimuli in the brain of *Xenopus* tadpoles. We suggest that the dynamic activation of distributed neural networks in the tectum can mediate stimulus categorisation in the early phases of sensorimotor transformation in this animal. We demonstrate that synaptic inhibition, although highly correlated with excitation, improves tuning for behaviorally relevant stimuli in individual neurons, and also hypothesise that the ultimate role of inhibition in the tectum may be in maintaining the proper ratio of direct and recurrent activation in this structure.

Supporting Information

Additional supporting information can be found in the online version of this article:

Video S1. Fast avoidance maneuvers. A set of 'fast' avoidance maneuvers performed by a freely-swimming tadpole in response to a computer-generated black circle sent by an operator towards the animal (circle radius $r = 0.28$ cm; speed $v = 2.9$ cm/s). In this video intervals of waiting time between the trials were cut out. Note the rapid accelerations and sharp turns that the animal performs.

Video S2. Slow avoidance maneuvers. A set of 'slow' avoidance maneuvers performed by an animal in response to approaches by a larger and slower circle (circle radius $r = 0.56$ cm; speed $v = 1.4$ cm/s). Waiting time between the trials is cut out from this video. Note that accelerations of the animal are more subtle than for 'fast' avoidance, whereas turn angles are smaller.

Video S3. Partially immobilised preparation. An original video from a partially immobilised behavior experiment, slowed down from 100 to 30 frames/s. A periodical tail movement is interrupted by a 'tail-flick', which is followed by a transient increase in oscillation frequency, and then a gradual recovery of normal background swimming. Note that the gel, in which the animal is partially embedded, has the same optical density as water, and is invisible in the video. The optic fiber that was used for visual stimulation can be seen in the lower left part of the video.

Video S4. Visual stimulation. A sequence of four visual stimuli used in this study ('flash', 'ramp', 'grid', and 'crash') shown one after another without delays. The video shows the surface of the microfiber bundle that was normally brought against the lens of the tadpole eye.

Fig. S1. The dynamics of spiking responses in individual tectal cells in *Xenopus* tadpoles was highly variable, yet we did not observe distinct compact clusters, corresponding to functional cell types, as they are described in adult birds and mammals (Frost & Sun, 2004; Liu *et al.*, 2011). On this plot, every circle corresponds to one cell.

Acknowledgements

We thank Andrey Shabalin for advice on the statistical analysis; Joe Fetcho, Ron Stoop, Richard Wassersug and James Simmons for productive and inspirational discussions on the phenomena described in this article; Kara Pratt, Kendall Jensen, Hollis Cline, Edward Ruthazer and Kasper Podgorski for insightful critique of preliminary versions of this article, and all members of the Aizenman laboratory for their help. Support for this study was provided by the NSF-IOB Directorate, the National Eye Institute of the NIH and a Fox Foundation Fellowship for the Visual Sciences. The funders had no role in the study design, data collection and analysis, decision to publish, or preparation of the manuscript.

Abbreviations

ACSF, artificial cerebrospinal fluid; GABA, γ-aminobutyric acid; OT, optic tectum; P_{ANOVA}, ANOVA test; P_{Corr}, Student's test on the Pearson correlation coefficient; P_{MW}, Mann–Whitney test; P_W, Wilcoxon signed-rank test; RGC, retinal ganglion cell.

References

Aizenman, C.D. & Cline, H.T. (2007) Enhanced visual activity in vivo forms nascent synapses in the developing retinotectal projection. *J. Neurophysiol.*, **97**, 2949–2957.

© 2014 Federation of European Neuroscience Societies and John Wiley & Sons Ltd

Aizenman, C.D., Akerman, C.J., Jensen, K.R. & Cline, H.T. (2003) Visually driven regulation of intrinsic neuronal excitability improves stimulus detection in vivo. *Neuron*, **39**, 831–842.
Akerman, C.J. & Cline, H.T. (2007) Refining the roles of GABAergic signaling during neural circuit formation. *Trends Neurosci.*, **30**, 382–389.
Baranauskas, G., Svirskiene, N. & Svirskis, G. (2012) 20 Hz membrane potential oscillations are driven by synaptic inputs in collision-detecting neurons in the frog optic tectum. *Neurosci. Lett.*, **528**, 196–200.
Benjamini, Y. & Hochberg, Y. (1995) Controlling the false discovery rate – a practical and powerful approach to multiple testing. *J. Roy. Stat. Soc. B.*, **57**, 289–300.
Blackiston, D.J. & Levin, M. (2012) Aversive training methods in *Xenopus laevis*: general principles. *Cold Spring Harb. Protoc.*, doi: 10.1101/pdb.top068338. [Epub ahead of print].
Blackiston, D.J. & Levin, M. (2013) Inversion of left-right asymmetry alters performance of *Xenopus* tadpoles in nonlateralized cognitive tasks. *Anim. Behav.*, **86**, 459–466.
Bollmann, J.H. & Engert, F. (2009) Subcellular topography of visually driven dendritic activity in the vertebrate visual system. *Neuron*, **61**, 895–905.
Brainard, D.H. (1997) The psychophysics toolbox. *Spatial Vision*, **10**, 433–436.
Brecht, M., Goebel, R., Singer, W. & Engel, A.K. (2001) Synchronization of visual responses in the superior colliculus of awake cats. *NeuroReport*, **12**, 43–47.
Brembs, B. (2011) Towards a scientific concept of free will as a biological trait: spontaneous actions and decision-making in invertebrates. *P. Roy. Soc. Lond. B-Biol. Sci.*, **278**, 930–939.
Budick, S.A. & O'Malley, D.M. (2000) Locomotor repertoire of the larval zebrafish: swimming, turning and prey capture. *J. Exp. Biol.*, **203**, 2565–2579.
Burgess, H.A. & Granato, M. (2007) Sensorimotor gating in larval zebrafish. *J. Neurosci.*, **27**, 4984–4994.
Card, G.M. (2012) Escape behaviors in insects. *Curr. Opin. Neurobiol.*, **22**, 180–186.
Colwill, R.M. & Creton, R. (2011) Imaging escape and avoidance behavior in zebrafish larvae. *Rev. Neuroscience*, **22**, 63–73.
Das, S., Keller, E.L. & Arai, K. (1996) A distributed model of the saccadic system: the effects of internal noise. *Neurocomputing*, **11**, 245–269.
Deeg, K.E. & Aizenman, C.D. (2011) Sensory modality-specific homeostatic plasticity in the developing optic tectum. *Nat. Neurosci.*, **14**, 548–550.
Deeg, K.E., Sears, I.B. & Aizenman, C.D. (2009) Development of multisensory convergence in the *Xenopus* optic tectum. *J. Neurophysiol.*, **102**, 3392–3404.
Domenici, P. & Blake, R. (1997) The kinematics and performance of fish fast-start swimming. *J. Exp. Biol.*, **200**, 1165–1178.
Dong, W. & Aizenman, C.D. (2012) A competition-based mechanism mediates developmental refinement of tectal neuron receptive fields. *J. Neurosci.*, **32**, 16872–16879.
Dong, W., Lee, R.H., Xu, H., Yang, S., Pratt, K.G., Cao, V., Song, Y.K., Nurmikko, A. & Aizenman, C.D. (2009) Visual avoidance in *Xenopus* tadpoles is correlated with the maturation of visual responses in the optic tectum. *J. Neurophysiol.*, **101**, 803–815.
Dunfield, D. & Haas, K. (2009) Metaplasticity governs natural experience-driven plasticity of nascent embryonic brain circuits. *Neuron*, **64**, 240–250.
Ewert, J.P. (1997) Neural correlates of key stimulus and releasing mechanism: a case study and two concepts. *Trends Neurosci.*, **20**, 332–339.
Fetcho, J.R. (1991) Spinal network of the Mauthner cell. *Brain Behav. Evolut.*, **37**, 298–316.
Fetcho, J.R. & McLean, D.L. (2010) Some principles of organization of spinal neurons underlying locomotion in zebrafish and their implications. *Ann. NY Acad. Sci.*, **1198**, 94–104.
Foeller, E., Celikel, T. & Feldman, D.E. (2005) Inhibitory sharpening of receptive fields contributes to whisker map plasticity in rat somatosensory cortex. *J. Neurophysiol.*, **94**, 4387–4400.
Fotowat, H. & Gabbiani, F. (2011) Collision detection as a model for sensory-motor integration. *Annu. Rev. Neurosci.*, **34**, 1–19.
Frost, B.J. & Sun, H. (2004) The biological bases of time-to-collision computation. *Adv. Psychol.*, **135**, 13–37.
Gabbiani, F., Krapp, H.G., Hatsopoulos, N., Mo, C.H., Koch, C. & Laurent, G. (2004) Multiplication and stimulus invariance in a looming-sensitive neuron. *J. Physiology-Paris*, **98**, 19–34.
Gahtan, E., Sankrithi, N., Campos, J.B. & O'Malley, D.M. (2002) Evidence for a widespread brain stem escape network in larval zebrafish. *J. Neurophysiol.*, **87**, 608–614.
Goddard, C.A., Sridharan, D., Huguenard, J.R. & Knudsen, E.I. (2012) Gamma oscillations are generated locally in an attention-related midbrain network. *Neuron*, **73**, 567–580.
Grüsser, O.-J. & Grüsser-Cornehls, U. (1976) Neurophysiology of the anuran visual system. In Precht, W. & Llinas, R. (Eds), *Frog Neurobiology*. Springer, Berlin, Heidelberg, pp. 297–385.
Hale, M.E., Long, J.H., McHenry, M.J. & Westneat, M.W. (2002) Evolution of behavior and neural control of the fast-start escape response. *Evolution*, **56**, 993–1007.
Hentschke, H. & Stuttgen, M.C. (2011) Computation of measures of effect size for neuroscience data sets. *Eur. J. Neurosci.*, **34**, 1887–1894.
Herberholz, J. & Marquart, G.D. (2012) Decision making and behavioral choice during predator avoidance. *Front. Neurosci.*, **6**, 125.
Hiramoto, M. & Cline, H.T. (2009) Convergence of multisensory inputs in *Xenopus* tadpole tectum. *Dev. Neurobiol.*, **69**, 959–971.
Holt, C.E. & Harris, W.A. (1983) Order in the initial retinotectal map in *Xenopus* – a new technique for labeling growing nerve-fibers. *Nature*, **301**, 150–152.
House, D.R.C., EIstrott, J., Koh, E., Chung, J. & Feldman, D.E. (2011) Parallel regulation of feedforward inhibition and excitation during whisker map plasticity. *Neuron*, **72**, 819–831.
Huang, K.H., Ahrens, M.B., Dunn, T.W. & Engert, F. (2013) Spinal projection neurons control turning behaviors in zebrafish. *Curr. Biol.*, **23**, 1566–1573.
Ingle, D.J. & Hoff, K.V. (1990) Visually elicited evasive behavior in frogs. *Bioscience*, **40**, 284–291.
Isaacson, J.S. & Scanziani, M. (2011) How inhibition shapes cortical activity. *Neuron*, **72**, 231–243.
Ishikane, H., Kawana, A. & Tachibana, M. (1999) Short- and long-range synchronous activities in dimming detectors of the frog retina. *Visual Neurosci.*, **16**, 1001–1014.
Ishikane, H., Gangi, M., Honda, S. & Tachibana, M. (2005) Synchronized retinal oscillations encode essential information for escape behavior in frogs. *Nat. Neurosci.*, **8**, 1087–1095.
Jensen, M.S., Azouz, R. & Yaari, Y. (1994) Variant firing patterns in rat hippocampal pyramidal cells modulated by extracellular potassium. *J. Neurophysiol.*, **71**, 831–839.
Kang, H.J. & Li, X.H. (2010) Response properties and receptive field organization of collision-sensitive neurons in the optic tectum of bullfrog, *Rana catesbeiana*. *Neurosci. Bull.*, **26**, 304–316.
Karayannis, T., Elfant, D., Huerta-Ocampo, I., Teki, S., Scott, R.S., Rusakov, D.A., Jones, M.V. & Capogna, M. (2010) Slow GABA transient and receptor desensitization shape synaptic responses evoked by hippocampal neurogliaform cells. *J. Neurosci.*, **30**, 9898–9909.
Keil, M.S. & Lopez-Moliner, J. (2012) Unifying time to contact estimation and collision avoidance across species. *PLoS Comput. Biol.*, **8**, e1002625.
Khakhalin, A.S. & Aizenman, C.D. (2012) GABAergic transmission and chloride equilibrium potential are not modulated by pyruvate in the developing optic tectum of *Xenopus laevis* tadpoles. *PLoS One*, **7**, e34446.
King, J.G., Lettvin, J.Y. & Gruberg, E.R. (1999) Selective, unilateral, reversible loss of behavioral responses to looming stimuli after injection of tetrodotoxin or cadmium chloride into the frog optic nerve. *Brain Res.*, **841**, 20–26.
Kohashi, T. & Oda, Y. (2008) Initiation of Mauthner- or non-Mauthner-mediated fast escape evoked by different modes of sensory input. *J. Neurosci.*, **28**, 10641–10653.
Komban, S.J., Alonso, J.M. & Zaidi, Q. (2011) Darks are processed faster than lights. *J. Neurosci.*, **31**, 8654–8658.
Korn, H. & Faber, D.S. (2005) The Mauthner cell half a century later: a neurobiological model for decision-making? *Neuron*, **47**, 13–28.
Kuras, A., Baginskas, A. & Batuleviciene, V. (2006) Non-NMDA and NMDA receptors are involved in suprathreshold excitation of network of frog tectal neurons by a single retinal ganglion cell. *Neurosci. Res.*, **54**, 328–337.
Lamme, V.A. & Roelfsema, P.R. (2000) The distinct modes of vision offered by feedforward and recurrent processing. *Trends Neurosci.*, **23**, 571–579.
Lazar, G. (1973) The development of the optic tectum in *Xenopus laevis*: a Golgi study. *J. Anat.*, **116**, 347–355.
Lazar, G. & Szekely, G. (1967) Golgi studies on the optic center of the frog. *J. Hirnforsch.*, **9**, 329–344.
Lee, P. & Hall, W.C. (2006) An in vitro study of horizontal connections in the intermediate layer of the superior colliculus. *J. Neurosci.*, **26**, 4763–4768.

© 2014 Federation of European Neuroscience Societies and John Wiley & Sons Ltd

Lettvin, J.Y., Maturana, H.R., McCulloch, W.S. & Pitts, W.H. (1959) What the frog's eye tells the frog's brain. *P. IRE*, **47**, 1940–1951.
Liu, Y.J., Wang, Q. & Li, B. (2011) Neuronal responses to looming objects in the superior colliculus of the cat. *Brain Behav. Evolut.*, **77**, 193–205.
Medan, V. & Preuss, T. (2011) Dopaminergic-induced changes in Mauthner cell excitability disrupt prepulse inhibition in the startle circuit of goldfish. *J. Neurophysiol.*, **106**, 3195–3204.
Meredith, M.A. & Ramoa, A.S. (1998) Intrinsic circuitry of the superior colliculus: pharmacophysiological identification of horizontally oriented inhibitory interneurons. *J. Neurophysiol.*, **79**, 1597–1602.
Miraucourt, L.S., Silva, J.S., Burgos, K., Li, J., Abe, H., Ruthazer, E.S. & Cline, H.T. (2012) GABA expression and regulation by sensory experience in the developing visual system. *PLoS One*, **7**, e29086.
Mitchell, M. (1996) Computation in cellular automata: a selected review. In Schuster, H.G. & Gramss, T. (Eds), *Non-Standard Computation*. VCH Verlagsgesellschaft, Weinheim, pp. 95–140.
Munch, T.A., da Silveira, R.A., Siegert, S., Viney, T.J., Awatramani, G.B. & Roska, B. (2009) Approach sensitivity in the retina processed by a multifunctional neural circuit. *Nat. Neurosci.*, **12**, 1308–1316.
Nakagawa, H. & Hongjian, K. (2010) Collision-sensitive neurons in the optic tectum of the bullfrog, *Rana catesbeiana*. *J. Neurophysiol.*, **104**, 2487–2499.
Nieuwkoop, P.D. & Faber, J. (1994) *Normal Table of* Xenopus laevis *(Daudin): A Systematical and Chronological Survey of the Development from the Fertilized Egg Till the End of Metamorphosis*. Garland, New York.
Okun, M. & Lampl, I. (2008) Instantaneous correlation of excitation and inhibition during ongoing and sensory-evoked activities. *Nat. Neurosci.*, **11**, 535–537.
Orger, M.B., Kampff, A.R., Severi, K.E., Bollmann, J.H. & Engert, F. (2008) Control of visually guided behavior by distinct populations of spinal projection neurons. *Nat. Neurosci.*, **11**, 327–333.
Parker, R.O., McCarragher, B., Crouch, R. & Darden, A.G. (2010) Photoreceptor development in premetamorphic and metamorphic *Xenopus laevis*. *Anat. Rec.*, **293**, 383–387.
Pecka, M., Brand, A., Behrend, O. & Grothe, B. (2008) Interaural time difference processing in the mammalian medial superior olive: the role of glycinergic inhibition. *J. Neurosci.*, **28**, 6914–6925.
Peron, S. & Gabbiani, F. (2009a) Spike frequency adaptation mediates looming stimulus selectivity in a collision-detecting neuron. *Nat. Neurosci.*, **12**, 318–326.
Peron, S.P. & Gabbiani, F. (2009b) Role of spike-frequency adaptation in shaping neuronal response to dynamic stimuli. *Biol. Cybern.*, **100**, 505–520.
Perrins, R., Walford, A. & Roberts, A. (2002) Sensory activation and role of inhibitory reticulospinal neurons that stop swimming in hatchling frog tadpoles. *J. Neurosci.*, **22**, 4229–4240.
Person, A.L. & Raman, I.M. (2012) Purkinje neuron synchrony elicits time-locked spiking in the cerebellar nuclei. *Nature*, **481**, 502–505.
Podgorski, K., Dunfield, D. & Haas, K. (2012) Functional clustering drives encoding improvement in a developing brain network during awake visual learning. *PLoS Biol.*, **10**, e1001236.
Portugues, R. & Engert, F. (2009) The neural basis of visual behaviors in the larval zebrafish. *Curr. Opin. Neurobiol.*, **19**, 644–647.
Pratt, K.G. & Aizenman, C.D. (2007) Homeostatic regulation of intrinsic excitability and synaptic transmission in a developing visual circuit. *J. Neurosci.*, **27**, 8268–8277.
Pratt, K.G. & Aizenman, C.D. (2009) Multisensory integration in mesencephalic trigeminal neurons in *Xenopus* tadpoles. *J. Neurophysiol.*, **102**, 399–412.
Pratt, K.G. & Khakhalin, A.S. (2013) Modeling human neurodevelopmental disorders in the *Xenopus* tadpole: from mechanisms to therapeutic targets. *Dis. Model Mech.*, **6**, 1057–1065.
Pratt, K.G., Dong, W. & Aizenman, C.D. (2008) Development and spike timing-dependent plasticity of recurrent excitation in the *Xenopus* optic tectum. *Nat. Neurosci.*, **11**, 467–475.
Preuss, T. & Faber, D.S. (2003) Central cellular mechanisms underlying temperature-dependent changes in the goldfish startle-escape behavior. *J. Neurosci.*, **23**, 5617–5626.
Preuss, T., Osei-Bonsu, P.E., Weiss, S.A., Wang, C. & Faber, D.S. (2006) Neural representation of object approach in a decision-making motor circuit. *J. Neurosci.*, **26**, 3454–3464.
Reid, R.C. (2012) From functional architecture to functional connectomics. *Neuron*, **75**, 209–217.
Remy, S., Beck, H. & Yaari, Y. (2010) Plasticity of voltage-gated ion channels in pyramidal cell dendrites. *Curr. Opin. Neurobiol.*, **20**, 503–509.
Richards, B.A., Aizenman, C.D. & Akerman, C.J. (2010) In vivo spike-timing-dependent plasticity in the optic tectum of *Xenopus laevis*. *Front. Synaptic Neurosci.*, **2**, 7.
Richards, B.A., van Rheede, J.J. & Akerman, C.J. (2012) Visuospatial information in the retinotectal system of xenopus before correct image formation by the developing eye. *Dev. Neurobiol.*, **72**, 507–519.
Roberts, A., Hill, N.A. & Hicks, R. (2000) Simple mechanisms organise orientation of escape swimming in embryos and hatchling tadpoles of *Xenopus laevis*. *J. Exp. Biol.*, **203**, 1869–1885.
Royer, S., Zemelman, B.V., Losonczy, A., Kim, J., Chance, F., Magee, J.C. & Buzsaki, G. (2012) Control of timing, rate and bursts of hippocampal place cells by dendritic and somatic inhibition. *Nat. Neurosci.*, **15**, 769–775.
Shao, Y.R., Isett, B.R., Miyashita, T., Chung, J., Pourzia, O., Gasperini, R.J. & Feldman, D.E. (2013) Plasticity of recurrent L2/3 inhibition and gamma oscillations by whisker experience. *Neuron*, **80**, 210–222.
Shen, W., McKeown, C.R., Demas, J.A. & Cline, H.T. (2011) Inhibition to excitation ratio regulates visual system responses and behavior in vivo. *J. Neurophysiol.*, **106**, 2285–2302.
Shen, W., Liu, H.H., Schiapparelli, L., McClatchy, D., He, H.Y., Yates, J.R. 3rd & Cline, H.T. (2014) Acute synthesis of CPEB is required for plasticity of visual avoidance behavior in *Xenopus*. *Cell Rep.*, **6**, 737–747.
Shin, D.S., Yu, W., Fawcett, A. & Carlen, P.L. (2010) Characterizing the persistent CA3 interneuronal spiking activity in elevated extracellular potassium in the young rat hippocampus. *Brain Res.*, **1331**, 39–50.
Shin, D.S., Yu, W., Sutton, A., Calos, M. & Carlen, P.L. (2011) Elevated potassium elicits recurrent surges of large GABAA-receptor-mediated post-synaptic currents in hippocampal CA3 pyramidal neurons. *J. Neurophysiol.*, **105**, 1185–1198.
Simmons, P.J., Sztarker, J. & Rind, F.C. (2013) Looming detection by identified visual interneurons during larval development of the locust *Locusta migratoria*. *J. Exp. Biol.*, **216**, 2266–2275.
Steedman, J.G., Stirling, R.V. & Gaze, R.M. (1979) The central pathways of optic fibres in *Xenopus* tadpoles. *J. Embryol. Exp. Morph.*, **50**, 199–215.
Stitt, I., Galindo-Leon, E., Pieper, F., Engler, G. & Engel, A.K. (2013) Laminar profile of visual response properties in ferret superior colliculus. *J. Neurophysiol.*, **110**, 1333–1345.
Straka, H., Baker, R. & Gilland, E. (2001) Rhombomeric organization of vestibular pathways in larval frogs. *J. Comp. Neurol.*, **437**, 42–55.
Sun, Y.J., Wu, G.K., Liu, B.H., Li, P., Zhou, M., Xiao, Z., Tao, H.W. & Zhang, L.I. (2010) Fine-tuning of pre-balanced excitation and inhibition during auditory cortical development. *Nature*, **465**, 927–931.
Szepsenwol, J. (1935) L'existence de la cellule de MAUTHNER chez les amphibiens anoures. *C. R. Soc. Biol., Paris*, **87**, 944–946.
Tao, H.W. & Poo, M.M. (2005) Activity-dependent matching of excitatory and inhibitory inputs during refinement of visual receptive fields. *Neuron*, **45**, 829–836.
Tsuruyama, K., Hsiao, C.F. & Chandler, S.H. (2013) Participation of a persistent sodium current and calcium-activated non-specific cationic current to burst generation in trigeminal principal sensory neurons. *J. Neurophysiol.*, **110**, 1903–1914.
Vislay-Meltzer, R., Kampff, A.R. & Engert, F. (2006) Spatiotemporal specificity of neuronal activity directs the modification of receptive fields in the developing retinotectal system. *Neuron*, **50**, 101–114.
Vladimirov, N., Tu, Y. & Traub, R.D. (2012) Shortest loops are pacemakers in random networks of electrically coupled axons. *Front. Comput. Neurosci.*, **6**, 17.
Waldeck, R.F. & Gruberg, E.R. (1995) Studies on the optic chiasm of the leopard frog. I. Selective loss of visually elicited avoidance behavior after optic chiasm hemisection. *Brain Behav. Evolut.*, **46**, 84–94.
Wang, Y.C. & Frost, B.J. (1992) Time to collision is signaled by neurons in the nucleus rotundus of pigeons. *Nature*, **356**, 236–238.
Wassersug, R.J. & Yamashita, M. (2002) Assessing and interpreting lateralised behaviours in anuran larvae. *Laterality*, **7**, 241–260.
Wassersug, R.J., Naitoh, T. & Yamashita, M. (1999) Turning bias in tadpoles. *J. Herpetol.*, **33**, 543–548.
Wehr, M. & Zador, A.M. (2003) Balanced inhibition underlies tuning and sharpens spike timing in auditory cortex. *Nature*, **426**, 442–446.
Whitaker, K.W., Neumeister, H., Huffman, L.S., Kidd, C.E., Preuss, T. & Hofmann, H.A. (2011) Serotonergic modulation of startle-escape plasticity in an African cichlid fish: a single-cell molecular and physiological analysis of a vital neural circuit. *J. Neurophysiol.*, **106**, 127–137.

© 2014 Federation of European Neuroscience Societies and John Wiley & Sons Ltd

Wilent, W.B. & Contreras, D. (2005) Dynamics of excitation and inhibition underlying stimulus selectivity in rat somatosensory cortex. *Nat. Neurosci.*, **8**, 1364–1370.
Will, U. (1991) Amphibian Mauthner cells. *Brain Behav. Evolut.*, **37**, 317–332.
Wu, G., Malinow, R. & Cline, H.T. (1996) Maturation of a central glutamatergic synapse. *Science*, **274**, 972–976.
Wu, G.K., Arbuckle, R., Liu, B.H., Tao, H.W. & Zhang, L.I. (2008) Lateral sharpening of cortical frequency tuning by approximately balanced inhibition. *Neuron*, **58**, 132–143.
Xu, H., Khakhalin, A.S., Nurmikko, A.V. & Aizenman, C.D. (2011) Visual experience-dependent maturation of correlated neuronal activity patterns in a developing visual system. *J. Neurosci.*, **31**, 8025–8036.
Zhang, M., Liu, Y., Wang, S.Z., Zhong, W., Liu, B.H. & Tao, H.W. (2011) Functional elimination of excitatory feedforward inputs underlies developmental refinement of visual receptive fields in zebrafish. *J. Neurosci.*, **31**, 5460–5469.
Zhang, Y.F., Kim, I.J., Sanes, J.R. & Meister, M. (2012) The most numerous ganglion cell type of the mouse retina is a selective feature detector. *Proc. Natl. Acad. Sci. USA*, **109**, E2391–E2398.
Zhou, Y., Liu, B.H., Wu, G.Y.K., Kim, Y.J., Xiao, Z.J., Tao, H.Z.W. & Zhang, L.I. (2010) preceding inhibition silences layer 6 neurons in auditory cortex. *Neuron*, **65**, 706–717.
Zhu, J.J. & Lo, F.S. (2000) Recurrent inhibitory circuitry in the deep layers of the rabbit superior colliculus. *J. Physiol.*, **523**(Pt 3), 731–740.

© 2014 Federation of European Neuroscience Societies and John Wiley & Sons Ltd